Thermal conductivity of single-walled carbon nanotubes

Alexander V. Savin,[1,2] Bambi Hu,[3,4] and Yuri S. Kivshar[1]
[1]*Nonlinear Physics Centre, Research School of Physical Sciences and Engineering, The Australian National University, Canberra, Australian Capital Territory 0200, Australia*
[2]*Semenov Institute of Chemical Physics, Russian Academy of Sciences, Moscow 119991, Russia*
[3]*Department of Physics and Center for Nonlinear Studies, Hong Kong Baptist University, Hong Kong, China*
[4]*Department of Physics, University of Houston, Houston, Texas 77204-5005, USA*
(Received 25 January 2009; revised manuscript received 20 October 2009; published 30 November 2009)

We study numerically the thermal conductivity of single-walled carbon nanotubes for the cases of an isolated nanotube and a nanotube interacting with a substrate. We employ two different numerical methods: (i) direct modeling of the heat transfer by molecular-dynamics simulations and (ii) analysis of the equilibrium dynamics by means of the Green-Kubo formalism. For the numerical modeling of the effective interatomic interactions, we employ both the Brenner potentials and the intermolecular potentials used in the study of the dynamics of large macromolecules. We demonstrate that, quite independently of the methods employed and the potentials used, the character of the thermal conductivity depends crucially on the interaction between a nanotube and a substrate. While an isolated nanotube demonstrates *anomalous* thermal conductivity due to ballistic transport of long-wave acoustic phonons, the nanotube interacting with a flat substrate displays *normal* thermal conductivity due to both the appearance of a gap in the frequency spectrum of acoustic phonons and the absorption of long-wave acoustic phonons by the substrate. We study the dependence of the thermal conductivity on chirality, radius, and temperature of the single-walled carbon nanotubes in both the regimes and compare our findings with experimental data and earlier theoretical results for the thermal conductivity.

DOI: 10.1103/PhysRevB.80.195423 PACS number(s): 61.48.De, 65.80.+n, 63.22.Gh

I. INTRODUCTION

Carbon-based structures, such as diamond and graphite, demonstrate the largest measured thermal conductivity of any known material at moderate temperatures.[1] Since the discovery of carbon nanotubes in 1991,[2] it was suggested that this new material could have a thermal conductivity much larger than that of diamond and graphite.[3] Carbon nanotubes find a lot of applications in electronic and mechanical devices, therefore it is not surprising that the study of the properties of carbon nanotubes, including their heat transfer, has attracted a lot of attention over the past decade.[4,5]

Single-walled carbon nanotubes (SWCNTs) have sparked great scientific and engineering interest because of their relative simplicity along with their outstanding electrical and thermal properties. Consequently, SWCNTs were proposed for applications in integrated circuits as transistors or interconnects,[6] as well as in heat management as thermal interface materials.[7,8] In both of these cases, the knowledge of thermal properties of carbon nanotubes is a key for understanding their overall behavior.[9]

Experimental measurement of the dependence of the thermal conductivity coefficient on the carbon nanotube length is a difficult problem. However, several groups already reported results of such measurements.[9–17] The reported data differ by at least two orders of magnitude, namely, 290–25 000 W/mK, which suggests, on one hand, that the accuracy of such measurements is not high enough and, on the other hand, that the thermal conductivity depends on a number of factors, including the way a nanotube interacts with a substrate. In addition, there exist a large number of numerical studies of the thermal conductivity of nanotubes.[18–36] Unfortunately, these studies are somewhat inconsistent, and a number of issues are waiting to be fully clarified. For example, earlier papers studied very short nanotubes and therefore contained only intermediate values of the conductivity.[18,19,23,24] Later studies were concerned with longer nanotubes[20,22,25,26,28–30,33–35] and contain calculations of the dependence of the thermal conductivity coefficient on the nanotube length L. In particular, it was shown[20,22,25,28,35] that the coefficient grows as L^{α} with positive $\alpha>0$, which is consistent with the ballistic-diffusive mechanism of the thermal conductivity. The ballistic-diffusive regime of the thermal conductivity of carbon nanotubes was also suggested in Ref. 37, where the electric transport in a nanotube was studied experimentally. However, the opposite conclusion was reached in Ref. 38, where the length-dependent thermal conductivity of SWCNTs was measured for the case when the nanotube is placed on a Si substrate. In particular, it was observed that the coefficient of thermal conductivity saturates for larger values of the length L and approaches a constant value. This observation strongly contradicts the results of the molecular-dynamics simulations.[20,22,25,35] As a matter of fact, we should note here that such a comparison of theoretical results and experimental data seems hardly appropriate because in the experiment[38] SWCNTs were placed on a substrate while the theory was developed for isolated nanotubes. Therefore, a natural question arises: what is the effect of the substrate on the thermal conductivity of carbon nanotubes? To the best of our knowledge, this problem has never been addressed before.

All the papers devoted to the study of the thermal conductivity of nanotubes employed the so-called Brenner potential for the numerical modeling of the nanotube oscillatory dynamics. Many papers used the direct numerical studies of the heat transfer, whereas in Refs. 24, 26, and 32 the authors found the coefficient of the thermal conductivity by means of

the equilibrium molecular dynamics and the Green-Kubo formula but considered relatively short nanotubes. The purpose of this paper is twofold. First, we study numerically the thermal conductivity of isolated SWCNTs by applying two different methods and considering two types of the interaction potential to obtain detailed information on the dependence of the thermal conductivity coefficient on the length of the nanotube. Second, we analyze the effect of a flat substrate on thermal conductivity of a nanotube. In order to verify our results, we use the Brenner potential as well as simpler standard potentials of the intermolecular interaction which are used in the molecular-dynamics modeling of large macromolecules. Two different approaches are employed to characterize the thermal conductivity: (i) the direct modeling of the heat transfer by molecular-dynamics simulations and (ii) the use of the equilibrium molecular dynamics and the Green-Kubo formalism. To evaluate the effect of the nanotube structure, we study the nanotubes of very different geometries such as the nanotubes with chiralities $(m,0)$ (zigzag carbon nanotube) and (m,m) (armchair carbon nanotube). For different geometries of a nanotube, we analyze how its attachment to a substrate changes the thermal conductivity.

By employing numerical studies of the classical model of a nanotube, we demonstrate that the use of any of the two types of the interatomic potential produces similar results. An isolated infinite ideal nanotube demonstrates anomalous thermal conductivity due to ballistic flux of long-wave acoustic phonons, as was already reported in other studies. The coefficient of the thermal conductivity κ grows with the nanotube length L following the power-law dependence for large L, $\kappa \sim L^{\beta}$ with positive β. The heat flux autocorrelation function $C(t)$ in accord with the power dependence $C(t) \sim t^{\alpha}$ for $t \to \infty$, where $0 < \alpha < 1$. The exponents α and β depend only on the nanotube radius R but not on its chirality. For larger R, the value of α grows while β decreases. Modeling of the dependence of the thermal conductivity on the temperature has shown that the carbon nanotube demonstrates a similar anomalous thermal conductivity for all temperatures in the range $T \leq 500$ K.

A nanotube interacting with a substrate changes the character of its thermal conductivity, so that the conductivity becomes finite, in a sharp contrast with the case of an isolated nanotube. This effect is related to the fact that the interaction of the nanotube with a substrate destroys the ballistic propagation of long-wave phonons. First, the coupling of the nanotube to the substrate leads to the appearance of a narrow gap at the bottom of the frequency spectrum of small-amplitude oscillations (i.e., long-wave acoustic phonons become optical). Second, interaction of atoms of the nanotube with substrate atoms reduces the propagation length of phonons due to their absorption by the substrate. We believe that this physical picture and the results presented in this paper resolve the controversies between the experimental data obtained for the length-dependent thermal conductivity of individual SWCNTs on a Si substrate[38] and the results of earlier numerical simulations.[20,22,25,35]

The paper is organized as follows. In Sec. II we introduce our model and discuss our choice of interaction potentials and physical parameters used below in the numerical simulations of the SWCNT dynamics. Section III is devoted to the analysis of the linearized equations of motion and the properties of the corresponding dispersion relations for the linear waves. In particular, we analyze all types of linear modes, find their characteristic frequencies and velocities, and also define the density of the frequency spectrum of linear oscillations of the nanotubes. In Sec. IV we outline the numerical methods which we employ for analyzing the thermal conductivity of SWCNTs, including the calculation of the coefficient of the thermal conductivity and the heat flux through a SWCNT cross section. In addition, we discuss how to calculate numerically the heat flux autocorrelation function and its dependence on the linear wave dispersion. Section V summarizes our numerical results for two cases: an isolated nanotube and the nanotube placed on and interacting with a substrate. In particular, we calculate and discuss the dependence of the thermal conductivity coefficient on the length of SWCNT and also study the decay of the heat flux autocorrelation function for $t \to \infty$. In Sec. VI we compare our numerical results with the experimental data available in the literature, while in Sec. VII we summarize all major numerical results previously obtained in the modeling of the heat transport and thermal conductivity in nanotubes and discuss the differences and similarities with our results. Finally, Sec. VIII concludes the paper with a brief summary of our major findings.

II. MODEL OF A SINGLE-WALLED CARBON NANOTUBE

Our goal is to study numerically the heat transfer and the thermal conductivity of ideal long SWCNTs. For simplicity, we consider the nanotubes with the chirality indices $(m,0)$ (the so-called zigzag nanotubes) and (m,m) (the so-called armchair nanotubes). Figure 1 schematically shows the nanotube structures. From the geometrical point of view, these two types of nanotubes differ substantially, so we expect that our study would allow us to draw some conclusions about the effect of chirality on the thermal conductivity as well as on other physical properties. In principle, all the methods discussed in this paper can be applied to study the thermal conductivity in any type of nanotube with the chirality index (m,n).

A. Nanotube structure

We consider a carbon nanotube as a cylinder created from a sheet of graphite. It is convenient to describe the structure of an ideal nanotube as that created by the operation of a screw rotation by an elementary unit cell defined between two neighboring atoms of carbon placed on a surface of a tube. The corresponding operator, defined as $S(\Delta z, \delta\varphi)$, transforms a point with the cylindrical coordinates (z,φ) into the point with the cylindrical coordinates $(z+\Delta z, \varphi+\delta\varphi)$, i.e., it produces a shift along the axis by the distance Δz and a rotation by the angle $\delta\varphi$. This operation is commutative, i.e., any two operators, say $S_1 = S(\Delta z_1, \delta\varphi_1)$ and $S_2 = S(\Delta z_2, \delta\varphi_2)$, are linearly independent. Therefore, the operation $S_1^m S_2^n$ produces the coordinate transformation in accordance with the relation $(z,\varphi) \to (z+m\Delta z_1 + n\Delta z_2, \varphi + m\delta\varphi_1 + n\delta\varphi_2)$. The minimum values of the non-negative numbers m and n,

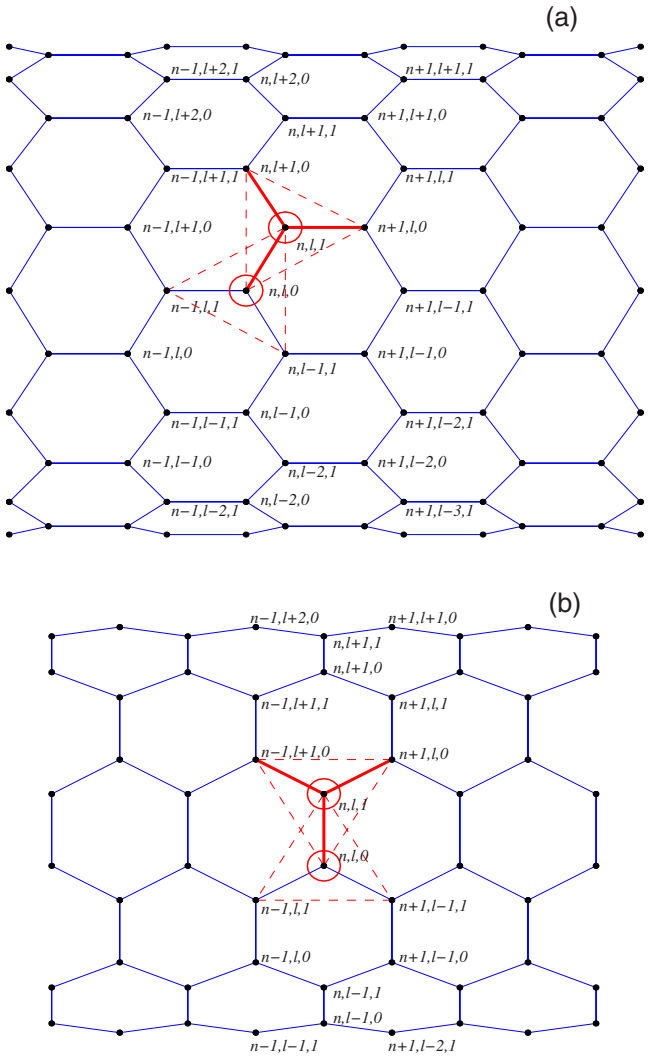

FIG. 1. (Color online) Schematic of a carbon nanotube with the chirality indices: (a) $(m,0)$ (zigzag SWCNT) and (b) (m,m) (armchair SWCNT) and the numbering of atoms. Thick red (gray) lines mark the valent bond couplings, red (gray) arcs mark the valent angle couplings, and thin dashed lines show the foundation of two pyramids which form a dihedral angle along the valent bonds in the elementary cell (n,l).

which reduce the corresponding operator to the unit operator, are called the nanotube indices and define the nanotube chirality. For the nanotubes with the chirality index $(m,0)$ (the so-called zigzag nanotubes) shown in Fig. 1(a), the first operator S_1 is reduced to the rotation by the angle $\delta\varphi_1 = 2\pi/m$ (and $\Delta z_1 = 0$) and the second operator S_2 defines a shift by the value $\Delta z_2 > 0$ and the rotation by the angle $\delta\varphi_2 = \pi/m$. For the nanotube with the chirality index (m,m) shown in Fig. 1(b), the first operator produces the rotation by the angle $\delta\varphi_1 = 2\pi/m (\Delta z_1 = 0)$ and the second operator produces a shift by the value $\Delta z_2 > 0$ and the rotation by the angle $\delta\varphi_2 = \pi/m$. Therefore, each atom of the carbon nanotube can be numbered by three indices (n,l,k), where the first two indices $n = 0, \pm 1, \pm 2, \ldots$ and $l = 0, 1, \ldots, m-1$ define the number of the elementary cell [the cell with the number (n,l) is obtained from the cell (0,0) by applying the operator $S_1^l S_2^n$] and the third index defines the number of the atoms in the cell, $k = 0, 1$.

Figure 1(a) shows the structure of a nanotube with the chirality index $(m,0)$. In an equilibrium state, the nanotube is defined by the following parameters: radius R_0 and two steps, h_1 and h_2. Each atom of the nanotube can be numbered by three indices (n,l,k), and the equilibrium coordinates of the atoms are define as

$$x^0_{n,l,0} = \Delta h(n-1), \quad x^0_{n,l,1} = \Delta h(n-1) + h_1,$$

$$y^0_{n,l,0} = R\cos(\phi_{n,l,0}), \quad y^0_{n,l,1} = R\cos(\phi_{n,l,1}),$$

$$z^0_{n,l,0} = R\sin(\phi_{n,l,0}), \quad z^0_{n,l,1} = R\sin(\phi_{n,l,1}), \tag{1}$$

where $\Delta h = h_1 + h_2$ is the longitudinal shift of the nanotube, $\Delta\phi = 2\pi/m$ is the angular step,

$$\phi_{n,l,0} = [l - 1 + (n-1)/2]\Delta\phi,$$

$$\phi_{n,l,1} = \phi_{n,l,0} + \Delta\phi/2 = [l - 1 + n/2]\Delta\phi.$$

Figure 1(b) shows the structure of a nanotube with the chirality index (m,m). The nanotube structure is described by the following parameters: radius R_0, angular shift φ_0, and longitudinal shift step h. In the equilibrium state, the atoms have the coordinates,

$$x^0_{n,l,0} = h(n-1), \quad x^0_{n,l,1} = h(n-1),$$

$$y^0_{n,l,0} = R\cos(\phi_{n,l,0}), \quad y^0_{n,l,1} = R\cos(\phi_{n,l,1}),$$

$$z^0_{n,l,0} = R\sin(\phi_{n,l,0}), \quad z^0_{n,l,1} = R\sin(\phi_{n,l,1}), \tag{2}$$

where $\phi_{n,l,0} = [l-1+(n-1)/2]\Delta\phi$ and $\phi_{n,l,1} = \phi_{n,l,0} + \varphi$ are the cylindrical angles and $\Delta\phi = 2\pi/m$.

B. Interatomic potentials

We write down the Hamiltonian for a nanotube in the following form:

$$H = \sum_n \sum_{l=0}^{m-1} \left[\frac{1}{2} M(\dot{\mathbf{u}}^2_{n,l,0} + \dot{\mathbf{u}}^2_{n,l,1}) + P_{n,l} \right], \tag{3}$$

where $M = 12(1.6603 \times 10^{-27})$ kg is the mass of a carbon atom and $\mathbf{u}_{n,l,k} = [x_{n,l,k}(t), y_{n,l,k}(t), z_{n,l,k}(t)]$ is the radius-vector describing the displacement of the carbon atom numbered by a set of indices (n,l,k) from its equilibrium position at the time t. The last term $P_{n,l}$ stands for the energy of interaction of the cell with the indices (n,l) with the atoms of the neighboring cells.

Almost all the papers devoted to the numerical study of the thermal properties of carbon nanotubes modeled the effective interatomic interaction by means of the Brenner potential.[39,40] In order to define the energy of interaction of two carbon atoms with the vector indices **i** and **j**, we need to know the positions of other carbon atoms coupled to them. Let us assume that $r_{\mathbf{ij}}$ is the distance between the atoms and $\theta_{\mathbf{i},1}$, $\theta_{\mathbf{i},2}$, and $\theta_{\mathbf{j},1}$, $\theta_{\mathbf{j},2}$ are the planar angles between the valent bonds (see the definitions in Fig. 2). Then the interaction energy can be written in the form

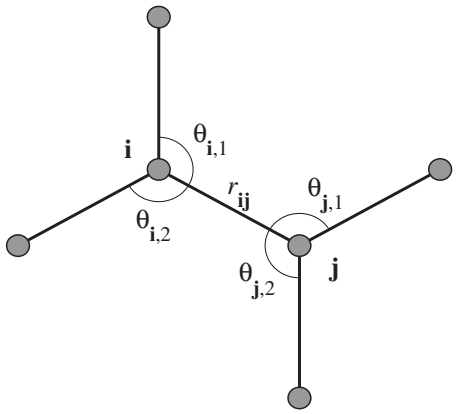

FIG. 2. Geometry of the carbon structure near the valent bond connecting the carbon atoms with the indices **i** and **j**.

$$U_{\mathbf{ij}} = V_R(r_{\mathbf{ij}}) - \tfrac{1}{2}(B_{\mathbf{ij}} + B_{\mathbf{ji}})V_A(r_{\mathbf{ij}}), \tag{4}$$

where

$$V_R(r) = \frac{D}{S-1}\exp[-\sqrt{2S}\beta(r-r_0)]$$

is the repulsive part of the interaction potential,

$$V_A(r) = \frac{DS}{S-1}\exp[-\sqrt{2/S}\beta(r-r_0)]$$

is the attractive part of the interaction potential,

$$B_{\mathbf{ij}} = [1 + G(\theta_{\mathbf{i},1}) + G(\theta_{\mathbf{i},2})]^{-\delta},$$

$$B_{\mathbf{ji}} = [1 + G(\theta_{\mathbf{j},1}) + G(\theta_{\mathbf{j},2})]^{-\delta},$$

and the function $G(\theta)$ is defined as follows:

$$G(\theta) = a_0\left[1 + \frac{c_0^2}{d_0^2} - \frac{c_0^2}{d_0^2 + (1+\cos\theta)^2}\right].$$

We employ two sets of the physical parameters in this model, namely, the set[39] introduced earlier and defined as

$$r_0 = 1.315\ \text{Å}, \quad D = 6.325\ \text{eV}, \quad \beta = 1.5\ \text{Å}^{-1},$$

$$S = 1.29, \quad a_0 = 0.011\ 304, \quad c_0 = 19,$$

$$d_0 = 2.5, \quad \delta = 0.804\ 69 \tag{5}$$

and the so-called improved set of the physical parameters,[31,40]

$$r_0 = 1.39\ \text{Å}, \quad D = 6.0\ \text{eV}, \quad \beta = 2.1\ \text{Å}^{-1},$$

$$S = 1.22, \quad a_0 = 0.000\ 208\ 13, \quad c_0 = 330,$$

$$d_0 = 3.5, \quad \delta = 0.5. \tag{6}$$

When the Brenner potential is used [Eq. (4)], the interaction energy for two neighboring cells can be presented in the following forms:

$$P_{n,l} = U_{(n,l,0),(n,l,1)} + U_{(n,l,1),(n+1,l,0)} + U_{(n,l,1),(n,l+1,0)}$$

for the nanotube with the chirality index $(m,0)$ and

$$P_{n,l} = U_{(n,l,0),(n,l,1)} + U_{(n,l,1),(n+1,l,0)} + U_{(n,l,1),(n-1,l+1,0)}$$

for the nanotube with the chirality index (m,m) (see Fig. 1).

The Brenner potential allows us to model the formation and breakup of molecular structures, as well as breakdown and formation of valent bonds. However, since for the temperatures $T \leq 400$ K the nanotube structure does not change, we can also employ simpler standard potentials for the intermolecular interaction which have already been used in the molecular-dynamics simulations of large macromolecules.[41–43] In this case, the interaction energy can be presented in the following forms:

$$\begin{aligned}
P_{n,l} = {} & V(\mathbf{u}_{n,l,0},\mathbf{u}_{n,l,1}) + V(\mathbf{u}_{n,l,1},\mathbf{u}_{n+1,l,0}) + V(\mathbf{u}_{n,l,1},\mathbf{u}_{n,l+1,0}) \\
& + U(\mathbf{u}_{n-1,l,1},\mathbf{u}_{n,l,0},\mathbf{u}_{n,l-1,1}) + U(\mathbf{u}_{n-1,l,1},\mathbf{u}_{n,l,0},\mathbf{u}_{n,l,1}) \\
& + U(\mathbf{u}_{n,l-1,1},\mathbf{u}_{n,l,0},\mathbf{u}_{n,l,1}) + U(\mathbf{u}_{n,l,0},\mathbf{u}_{n,l,1},\mathbf{u}_{n,l+1,0}) \\
& + U(\mathbf{u}_{n,l,0},\mathbf{u}_{n,l,1},\mathbf{u}_{n+1,l,0}) + U(\mathbf{u}_{n,l+1,0},\mathbf{u}_{n,l,1},\mathbf{u}_{n+1,l,0}) \\
& + W(\mathbf{u}_{n,l,1},\mathbf{u}_{n,l,0},\mathbf{u}_{n-1,l,1},\mathbf{u}_{n,l-1,1}) \\
& + W(\mathbf{u}_{n,l,1},\mathbf{u}_{n,l,0},\mathbf{u}_{n,l-1,1},\mathbf{u}_{n-1,l,1}) \\
& + W(\mathbf{u}_{n-1,l,1},\mathbf{u}_{n,l,0},\mathbf{u}_{n,l,1},\mathbf{u}_{n-1,l,1}) \\
& + W(\mathbf{u}_{n,l,0},\mathbf{u}_{n,l,1},\mathbf{u}_{n,l+1,0},\mathbf{u}_{n+1,l,0}) \\
& + W(\mathbf{u}_{n,l,0},\mathbf{u}_{n,l,1},\mathbf{u}_{n+1,l,0},\mathbf{u}_{n,l+1,0}) \\
& + W(\mathbf{u}_{n+1,l,0},\mathbf{u}_{n,l,1},\mathbf{u}_{n,l,0},\mathbf{u}_{n,l+1,0})
\end{aligned} \tag{7}$$

for the nanotubes with the chirality index $(m,0)$ and

$$\begin{aligned}
P_{n,l} = {} & V(\mathbf{u}_{n,l,0},\mathbf{u}_{n,l,1}) + V(\mathbf{u}_{n,l,1},\mathbf{u}_{n+1,l,0}) + V(\mathbf{u}_{n,l,1},\mathbf{u}_{n-1,l+1,0}) \\
& + U(\mathbf{u}_{n-1,l,1},\mathbf{u}_{n,l,0},\mathbf{u}_{n+1,l-1,1}) + U(\mathbf{u}_{n-1,l,1},\mathbf{u}_{n,l,0},\mathbf{u}_{n,l,1}) \\
& + U(\mathbf{u}_{n+1,l-1,1},\mathbf{u}_{n,l,0},\mathbf{u}_{n,l,1}) + U(\mathbf{u}_{n,l,0},\mathbf{u}_{n,l,1},\mathbf{u}_{n-1,l+1,0}) \\
& + U(\mathbf{u}_{n,l,0},\mathbf{u}_{n,l,1},\mathbf{u}_{n+1,l,0}) + U(\mathbf{u}_{n-1,l+1,0},\mathbf{u}_{n,l,1},\mathbf{u}_{n+1,l,0}) \\
& + W(\mathbf{u}_{n,l,1},\mathbf{u}_{n,l,0},\mathbf{u}_{n-1,l,1},\mathbf{u}_{n+1,l-1,1}) \\
& + W(\mathbf{u}_{n,l,1},\mathbf{u}_{n,l,0},\mathbf{u}_{n+1,l-1,1},\mathbf{u}_{n-1,l,1}) \\
& + W(\mathbf{u}_{n-1,l,1},\mathbf{u}_{n,l,0},\mathbf{u}_{n,l,1},\mathbf{u}_{n+1,l-1,1}) \\
& + W(\mathbf{u}_{n,l,0},\mathbf{u}_{n,l,1},\mathbf{u}_{n-1,l+1,0},\mathbf{u}_{n+1,l,0}) \\
& + W(\mathbf{u}_{n,l,0},\mathbf{u}_{n,l,1},\mathbf{u}_{n+1,l,0},\mathbf{u}_{n-1,l+1,0}) \\
& + W(\mathbf{u}_{n+1,l,0},\mathbf{u}_{n,l,1},\mathbf{u}_{n,l,0},\mathbf{u}_{n-1,l+1,0})
\end{aligned} \tag{8}$$

for the nanotubes with the chirality index (m,m) (see Fig. 1). Here the first term $V(\mathbf{u}_1,\mathbf{u}_2)$ describes the deformation energy due to direct interaction between pairs of atoms with the coordinates $\mathbf{u}_1$ and $\mathbf{u}_2$. The second term $U(\mathbf{u}_1,\mathbf{u}_2,\mathbf{u}_3)$ describes the deformation energy of the angle between the bonds $\mathbf{u}_1\mathbf{u}_2$ and $\mathbf{u}_2\mathbf{u}_3$. Finally, the third term $W(\mathbf{u}_1,\mathbf{u}_2,\mathbf{u}_3,\mathbf{u}_4)$ describes the deformation energy associated with a change of the effective angle between the planes $\mathbf{u}_1\mathbf{u}_2\mathbf{u}_3$ and $\mathbf{u}_2\mathbf{u}_3\mathbf{u}_4$.

First, we consider the potentials employed in the modeling of the dynamics of large macromolecules[44–46] for the valent bond coupling,

TABLE I. Dependence of the nanotube radius R, longitudinal steps h_1 and h_2, velocities of torsion v_t and longitudinal v_l sounds, maximum (cutoff) frequency of small-amplitude oscillations ω_m on the chirality index m of the nanotube $(m,0)$ calculated for the molecular-dynamics potential [Eq. (8)], and the Brenner potential with the original [Eqs. (5)] and modified [Eqs. (6)] sets of physical parameters, respectively.

m	R (Å)	h_1 (Å)	h_2 (Å)	v_t (m/s)	v_l (m/s)	ω_m (cm^{-1})
5	2.0011	0.69373	1.41800	8536	13754	1685
	2.0334	0.70026	1.42303	9259	13609	1221
	2.0761	0.71096	1.45422	10624	16666	1655
10	3.9274	0.70774	1.41800	8004	13744	1609
	3.9528	0.70571	1.42062	9263	14245	1260
	4.0386	0.72030	1.45177	10691	17644	1699
20	7.8261	0.70895	1.41800	7824	13610	1603
	7.8459	0.70863	1.41975	9253	14409	1272
	8.0179	0.72400	1.45096	10699	17901	1713
100	39.091	0.70900	1.41800	7762	13522	1600
	39.133	0.70968	1.41946	9253	14457	1276
	39.994	0.72528	1.45069	10703	17964	1717

$$V(\mathbf{u}_1,\mathbf{u}_2) = D\{\exp[-\alpha(\rho-\rho_0)]-1\}^2, \quad \rho = |\mathbf{u}_2-\mathbf{u}_1|, \quad (9)$$

where $D=4.9632$ eV is the energy of the valent bond and $\rho_0=1.418$ Å is an equilibrium length of the bond; the potential of the valent angle

$$U(\mathbf{u}_1,\mathbf{u}_2,\mathbf{u}_3) = \epsilon_v(\cos\varphi-\cos\varphi_0)^2,$$

$$\cos\varphi = \frac{(\mathbf{u}_3-\mathbf{u}_2,\mathbf{u}_1-\mathbf{u}_2)}{|\mathbf{u}_3-\mathbf{u}_2|\cdot|\mathbf{u}_2-\mathbf{u}_1|}, \quad (10)$$

so that the equilibrium value of the angle is defined as $\cos\varphi_0=\cos(2\pi/3)=1/2$ and the potential of the torsion angle

$$W(\mathbf{u}_1,\mathbf{u}_2,\mathbf{u}_3,\mathbf{u}_4) = \epsilon_t(1-\cos\phi),$$

$$\cos\phi = (\mathbf{v}_1,\mathbf{v}_2)/(|\mathbf{v}_1|\cdot|\mathbf{v}_2|),$$

$$\mathbf{v}_1 = (\mathbf{u}_2-\mathbf{u}_1)\times(\mathbf{u}_3-\mathbf{u}_2),$$

$$\mathbf{v}_2 = (\mathbf{u}_3-\mathbf{u}_2)\times(\mathbf{u}_4-\mathbf{u}_3). \quad (11)$$

The specific values of the parameters $\alpha=1.7889$ $\mathrm{Å}^{-1}$, $\epsilon_v=1.3143$ eV, and $\epsilon_t=0.499$ eV are found from the frequency spectrum of small-amplitude oscillations of a sheet of graphite.[47]

III. DISPERSION AND SMALL-AMPLITUDE OSCILLATIONS

In order to find the ground (equilibrium) state of the nanotube with the chirality index $(m,0)$, we should minimize numerically the potential energy of the stationary homogeneous state [Eqs. (1)] with respect to the parameters h_1, h_2, and R, i.e.,

$$E_0 = \frac{1}{Nm}\sum_{n=1}^{N}\sum_{l=0}^{m-1} P_{n,l} \to \min_{R,h_1,h_2}. \quad (12)$$

To solve this minimization problem [Eq. (12)], we use the periodic boundary condition in the index n and also take $N=m$. Let us assume that a set of the parameters R, h_1, and h_2 satisfies this minimization problem, then the energy $E_0>0$ corresponding to that solution defines the energy of the ground state. In what follows, we will calculate the nanotube energy from this ground state value.

For the nanotube with the chirality index (m,m), we should make the minimization of the potential energy [Eqs. (2)] with respect to the parameters R, φ, and h. All specific values of the geometric parameters of the nanotubes for different values of the index m are summarized in Table I.

A. Dispersion relations

For the analysis of small-amplitude oscillations of the nanotube with the chirality index $(m,0)$, we employ the local cylindrical coordinates $u_{n,l,k}$, $v_{n,l,k}$, and $w_{n,l,k}$ defined as

$$x_{n,l,k} = x^0_{n,l,k} + u_{n,l,k},$$

$$y_{n,l,k} = y^0_{n,l,k} - v_{n,l,k}\sin\phi_{n,l,k} + w_{n,l,k}\cos\phi_{n,l,k},$$

$$z_{n,l,k} = z^0_{n,l,k} + v_{n,l,k}\cos\phi_{n,l,k} + w_{n,l,k}\sin\phi_{n,l,k}, \quad (13)$$

where $\phi_{n,l,0}=[l-1+(n-1)/2]\Delta\phi$ and $\phi_{n,l,1}=[l-1+n/2]\Delta\phi$. The center of this local system of coordinates coincides with the equilibrium position of the atom (n,l,k) ($n=0,\pm1,\pm2,\ldots$; $l=0,1,\ldots,m-1$; $k=0,1$). The first coordinate $u_{n,l,k}$ defines the longitudinal direction along the nanotube, the second coordinate $v_{n,l,k}$ defines the direction tangential to the cross section of the nanotube, while the coordinate $w_{n,l,k}$ defines the direction orthogonal to the cyl-

inder surface. In this new system of coordinates, the Hamiltonian takes the form

$$H = \sum_{n} \sum_{l=0}^{m-1} \left\{ \frac{1}{2} M(\dot{\mathbf{v}}_{n,l}, \dot{\mathbf{v}}_{n,l}) + \mathcal{P}(\mathbf{v}_{n-1,l}; \mathbf{v}_{n,l-1}; \mathbf{v}_{n,l}; \mathbf{v}_{n,l+1}; \mathbf{v}_{n+1,l}) \right\}, \quad (14)$$

where the six-dimensional vector $\mathbf{v}_{n,l}$ is defined as $\mathbf{v}_{n,l}=(u_{n,l,0}, v_{n,l,0}, w_{n,l,0}, u_{n,l,1}, v_{n,l,1}, w_{n,l,1})$ and function $\mathcal{P}(\mathbf{v}_{n-1,l}; \mathbf{v}_{n,l-1}; \mathbf{v}_{n,l}; \mathbf{v}_{n,l+1}; \mathbf{v}_{n+1,l}) = P(\mathbf{x}_{n-1,l}; \mathbf{x}_{n,l-1}; \mathbf{x}_{n,l}; \mathbf{x}_{n,l+1}; \mathbf{x}_{n+1,l})$, with vector $\mathbf{x}_{n,l}=(x_{n,l,0}, y_{n,l,0}, z_{n,l,0}, x_{n,l,1}, y_{n,l,1}, z_{n,l,1})$.

Hamiltonian (14) generates the following set of the equations of motion:

$$-M\ddot{\mathbf{v}}_{n,l} = F_{n,l}, \quad (15)$$

$$\begin{aligned} F_{n,l} = {} & \mathcal{P}_{\mathbf{v}_1}(\mathbf{v}_{n,l}; \mathbf{v}_{n+1,l-1}; \mathbf{v}_{n+1,l}; \mathbf{v}_{n+1,l+1}; \mathbf{v}_{n+2,l}) \\ & + \mathcal{P}_{\mathbf{v}_2}(\mathbf{v}_{n-1,l+1}; \mathbf{v}_{n,l}; \mathbf{v}_{n,l+1}; \mathbf{v}_{n,l+2}; \mathbf{v}_{n+1,l+1}) \\ & + \mathcal{P}_{\mathbf{v}_3}(\mathbf{v}_{n-1,l}; \mathbf{v}_{n,l-1}; \mathbf{v}_{n,l}; \mathbf{v}_{n,l+1}; \mathbf{v}_{n+1,l}) \\ & + \mathcal{P}_{\mathbf{v}_4}(\mathbf{v}_{n-1,l-1}; \mathbf{v}_{n,l-2}; \mathbf{v}_{n,l-1}; \mathbf{v}_{n,l}; \mathbf{v}_{n+1,l+1}) \\ & + \mathcal{P}_{\mathbf{v}_5}(\mathbf{v}_{n-2,l}; \mathbf{v}_{n-1,l-1}; \mathbf{v}_{n-1,l}; \mathbf{v}_{n-1,l+1}; \mathbf{v}_{n,l}). \end{aligned} \quad (16)$$

In the linear approximation, this system takes the form

$$\begin{aligned} -M\ddot{\mathbf{v}}_{n,l} = {} & B_1\mathbf{v}_{n,l} + B_2\mathbf{v}_{n+1,l} + B_2^*\mathbf{v}_{n-1,l} + B_3\mathbf{v}_{n+2,l} + B_3^*\mathbf{v}_{n-2,l} \\ & + B_4\mathbf{v}_{n+1,l-1} + B_4^*\mathbf{v}_{n-1,l+1} + B_5\mathbf{v}_{n+1,l+1} + B_5^*\mathbf{v}_{n-1,l-1} \\ & + B_6\mathbf{v}_{n,l+1} + B_6^*\mathbf{v}_{n,l-1} + B_7\mathbf{v}_{n,l+2} + B_7^*\mathbf{v}_{n,l-2}, \end{aligned} \quad (17)$$

where the matrix elements are defined as

$$B_1 = \mathcal{P}_{\mathbf{v}_1\mathbf{v}_1} + \mathcal{P}_{\mathbf{v}_2\mathbf{v}_2} + \mathcal{P}_{\mathbf{v}_3\mathbf{v}_3} + \mathcal{P}_{\mathbf{v}_4\mathbf{v}_4} + \mathcal{P}_{\mathbf{v}_5\mathbf{v}_5},$$

$$B_2 = \mathcal{P}_{\mathbf{v}_1\mathbf{v}_3} + \mathcal{P}_{\mathbf{v}_3\mathbf{v}_5}, \quad B_3 = \mathcal{P}_{\mathbf{v}_1\mathbf{v}_5},$$

$$B_4 = \mathcal{P}_{\mathbf{v}_1\mathbf{v}_2} + \mathcal{P}_{\mathbf{v}_4\mathbf{v}_5}, \quad B_5 = \mathcal{P}_{\mathbf{v}_1\mathbf{v}_4} + \mathcal{P}_{\mathbf{v}_2\mathbf{v}_5},$$

$$B_6 = \mathcal{P}_{\mathbf{v}_2\mathbf{v}_3} + \mathcal{P}_{\mathbf{v}_3\mathbf{v}_4}, \quad B_7 = \mathcal{P}_{\mathbf{v}_2\mathbf{v}_4},$$

and the matrix of the partial derivatives takes the form

$$\mathcal{P}_{\mathbf{v}_i,\mathbf{v}j} = \frac{\partial^2 \mathcal{P}}{\partial \mathbf{v}_i \, \partial \mathbf{v}_j}(\mathbf{0},\mathbf{0},\mathbf{0},\mathbf{0},\mathbf{0}), \quad i,j = 1,2,3,4,5.$$

Solutions of the system of linear equation [Eq. (17)] can be sought in the standard form,

$$\mathbf{v}_{n,l} = A\mathbf{e}\,\exp(iqn + il\delta - i\omega t), \quad (18)$$

where A is the mode amplitude, $\mathbf{e}$ is the normalized vector ($|\mathbf{e}|=1$), $q \in [0,\pi]$ is the dimensionless wave number, and $\delta=2\pi j/m$, where $j=0,1,\ldots,m-1$, is the dimensionless momentum of phonons. Substituting expression (18) into system (17), we obtain the eigenvalue problem,

$$\begin{aligned} M\omega^2\mathbf{A} = {} & [B_1 + B_2e^{iq} + B_2^*e^{-iq} + B_3e^{2iq} + B_3^*e^{-2iq} + B_4e^{iq-i\delta} \\ & + B_4^*e^{-iq+i\delta} + B_5e^{iq+i\delta} + B_5^*e^{-iq-i\delta} + B_6e^{iq} + B_6^*e^{-i\delta} \\ & + B_7e^{2i\delta} + B_7^*e^{-2i\delta}]A. \end{aligned} \quad (19)$$

Therefore, in order to find the dispersion relations characterizing the modes of the nanotube, for each fixed value of the wave number $0 \le q \le \pi$ and fixed momentum δ, i.e., for each value of the index j, we need to find the eigenvalues of the Hermitian matrix [Eq. (19)] of the order 6×6. As a result, the dispersion curves are composed of $6m$ branches $\{\omega_{j,k}(q)\}_{j=0,k=1}^{m-1,6}$, as shown in Fig. 3.

Similarly, using the local coordinates [Eqs. (13)] with the cylindrical angles $\phi_{n,l,0}=[l-1+(n-1)/2]2\pi/m$ and $\phi_{n,l,1}=\phi_{n,l,0}^0+\varphi$, we can obtain all $6m$ branches of the dispersion curves $\{\omega_{j,k}(q)\}_{j=0,k=1}^{m-1,6}$ for the nanotube with the chirality index (m,m) (see Fig. 3).

As is seen in Fig. 3, the spectrum of the nanotube oscillations occupies the frequency interval $[0,\omega_m]$, where the maximum (cutoff) frequency ω_m practically does not depend on the chirality index m. When we use the standard molecular-dynamics potential [Eq. (8)], the maximum frequency is $\omega_m \approx 1600$ cm^{-1}. This value agrees well with the experimental data for a planar graphite.[48,49] The use of the Brenner potential with the original set of physical parameters [Eqs. (5)] gives much lower value, $\omega_m \approx 1250$ cm^{-1}. However, with the modified set of parameters the Brenner potential [Eqs. (6)] gives the more realistic value, $\omega_m \approx 1700$ cm^{-1}.

Now, we discuss the main features of the dispersion curves in more detail. For each value of the dimensionless parameter $\delta=2j\pi/m$, $j=0,1,\ldots,m-1$, the dispersion curves consists of six branches. Since the elementary cell of the nanotube consists of two atoms, these six branches can be divided into three optical and three acoustic branches. At $\delta=0$, two branches originate from the point $(q=0,\ \omega=0)$ (see Fig. 3). The first branch $\omega_{0,1}(q)$ describes torsion acoustic vibrations of the nanotubes, whereas the second branch $\omega_{0,2}(q)$ describes longitudinal acoustic oscillations of the nanotube. In this way, we define two sound speeds,

$$v_t = \Delta h \lim_{q\to 0} \frac{\omega_{0,1}(q)}{q}, \quad v_l = \Delta h \lim_{q\to 0} \frac{\omega_{0,2}(q)}{q},$$

where for the nanotube $(m,0)$ the longitudinal step is $\Delta h = h_1 + h_2$ and for the nanotube (m,m), this step is defined as $\Delta h = h$. The third branch $\omega_{0,3}(q)$ describes radial acoustic oscillations and the fourth branch $\omega_{0,4}(q)$ describes radial optical oscillations. The branch $\omega_{0,5}(q)$ corresponds to optical torsion oscillations, while the branch $\omega_{0,6}(q)$ describes optical longitudinal oscillations. The specific values of the sound speeds v_t and v_l are presented in Tables I and II.

At the first nonzero value of the momentum, $\delta=2\pi/m(j=1)$, the dispersion curves correspond to the nanotube oscillations with bending. The first dispersion curve $\omega_{1,1}(q)$ smoothly touches the zero line at $q=\pi/m$. At this particular value of q, ansatz (18) in the limit $\omega \to 0$ describes transverse displacements of the nanotube without deformations. Thus, here the first branch of the dispersion curves corresponds to the acoustic bending oscillations of the nanotube. Since two curves originate from the point $(\omega=0,\ q_m=\pi/m)$, the acoustic branch is double degenerated because the bending may occur in two orthogonal planes. The velocity of these bending oscillations is defined as

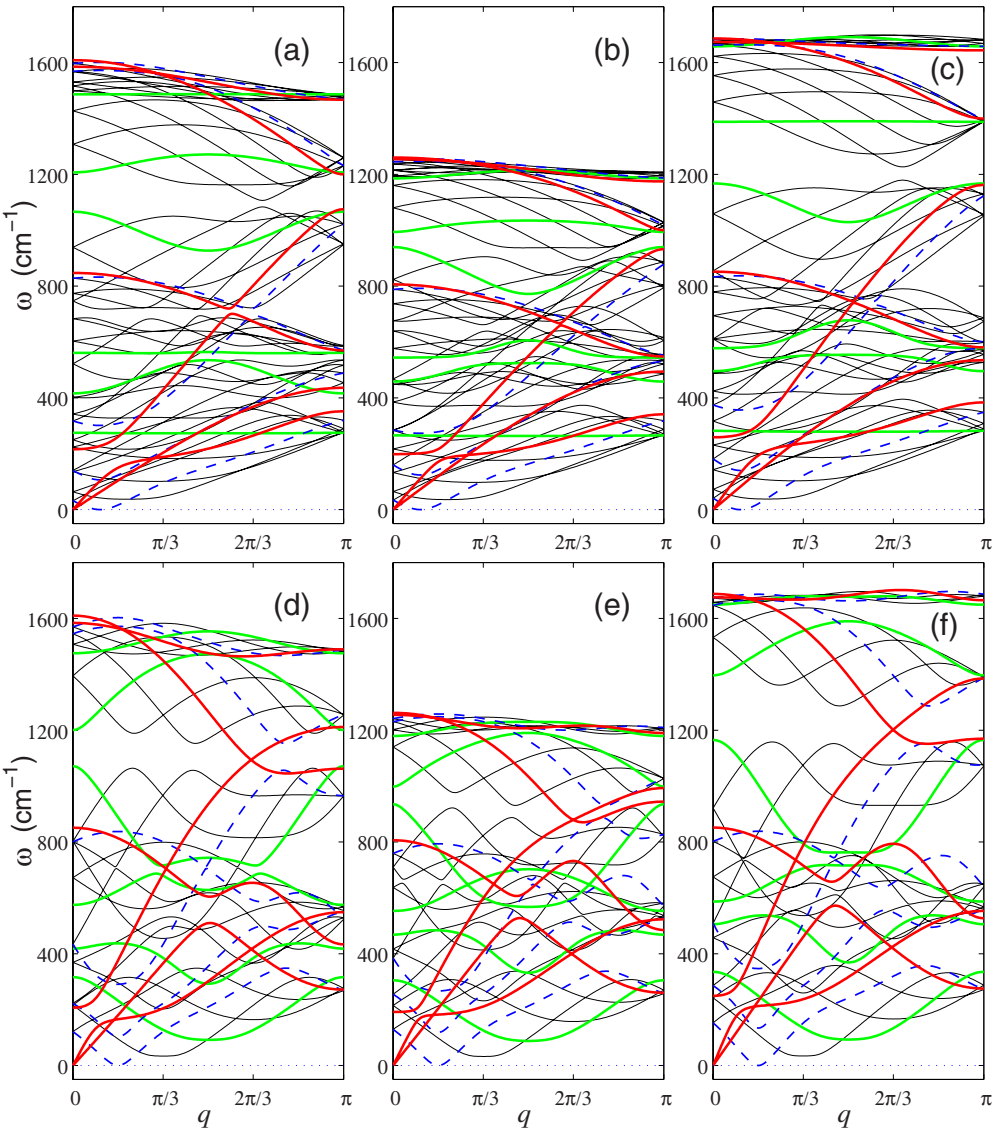

FIG. 3. (Color online) (a)–(c) Sixty dispersion curves of the (10,0) nanotube and (d)–(f) 36 dispersion curves of the (6,6) nanotube for (a) and (d) standard interatomic molecular-dynamics potential [Eq. (8)] and (b), (c), (e), and (f) Brenner potential with (b) and (e) original set of parameters [Eqs. (5)] and (c) and (f) modified parameters [Eqs. (6)]. Curves corresponding to phonons with zero momentum $\delta=0(j=0)$ are marked by red (dark gray), phonons with $\delta=2\pi/m(j=1)$ are marked by blue (dashed lines), and phonons with the momentum $\delta=\pi(j=m/2)$ are marked by green (light gray).

$$v_b = \Delta h \lim_{q\to 0} \omega_{1,1}(q_m + q)/q = 0.$$

Next, we analyze the linear oscillations of a nanotube with the momentum $\delta=\pi$ $(j=m/2)$ when the atoms of the neighboring elementary cells in the cross-section layer oscillate with the opposite phases. In this case, the dispersion curves for the chirality indices $(m,0)$ and (m,m) differ substantially. For the nanotube $(m,0)$, several dispersion curves are almost independent of q, which corresponds to a vanishing dispersion. Under such conditions, localized wave packets of such oscillations may have large lifetime, and nonlinearity can lead to the formation of stable strongly localized nonlinear modes, discrete breathers.[47] In the nanotube (m,m), the situation is different, and all modes are strongly dispersive. This specific difference will be seen below in the analysis of the heat flux autocorrelation function. The nanotube $(m,0)$, unlike the nanotube (m,m), corresponds to the correlation function with a slowly decaying oscillatory tail.

We would like to mention that, as follows from Fig. 3, the use of the Brenner potential with the modified set of physical parameters [Eqs. (6)] gives a very narrow frequency band of optical torsion oscillations of the nanotube. This seems to be an artifact of the Brenner potential and a contradiction to an experiment. Because of this narrow band, the wave packets corresponding to optical torsion oscillations will experience a very slow decay giving rise to slowly decaying high-frequency oscillations in the correlation function. Such oscillations decay rapidly provided the molecular-dynamics potential [Eq. (8)] is employed.

TABLE II. Dependence of the nanotube radius R, longitudinal step h, velocities of torsion v_t and longitudinal v_l sounds, maximum (cutoff) frequency of small-amplitude oscillations ω_m on the chirality index m of the nanotube (m,m) calculated for the molecular-dynamics potential [Eq. (8)], and the Brenner potential with the original [Eqs. (5)] and modified [Eqs. (6)] sets of physical parameters, respectively.

m	R (Å)	h (Å)	v_t (m/s)	v_l (m/s)	ω_m (cm^{-1})
3	2.0425	1.24018	7934	13914	1627
	2.0775	1.24370	8329	14190	1225
	2.1209	1.26877	9549	17482	1666
6	4.0639	1.23222	7887	13709	1610
	4.0894	1.23239	8996	14383	1262
	4.1782	1.25896	10387	17840	1702
12	8.1246	1.22918	7800	13589	1603
	8.1444	1.23002	9190	14444	1273
	8.3230	1.25695	10624	17947	1713
60	40.623	1.22807	7761	13464	1600
	40.666	1.22931	9251	14448	1276
	41.561	1.25635	10699	17916	1717

B. Density of states

Once the form of all branches of the dispersion relation $\{\omega_{j,k}(q)\}_{j=0,k=1}^{m-1,6}$ is known, we can determine the dimensionless density of states of the frequency spectrum, $p(\omega)$, normalized by the condition $\int_0^\infty p(\omega)d\omega=1$. The characteristic form of the density of frequency spectrum of linear modes is shown in Fig. 4.

We consider the density of states for the nanotubes (10,0) and (6,6) which have similar diameters but different structures. As is seen in Figs. 4(a) and 4(b), these two nanotubes have the same cutoff frequency $\omega_m=1610$ cm^{-1}, but the internal structures of the spectra differ substantially. For example, the nanotube (6,6) has a continuous spectrum, but the spectrum of the nanotube (10,0) includes two narrow gaps. The nanotube differs also by the number of singular points and their location. When the nanotube radius grows, these differences vanish. Indeed, the nanotubes (1000,0) and (600,600) demonstrate almost the same density of states [see Fig. 4(c)], which for the radius $R\approx 400$ Å coincides with the frequency spectrum density of the graphite.

Figure 4(c) shows the density of state of the carbon nanotube (600,600) calculated by using the molecular-dynamics potential [Eq. (8)] and the Brenner potential with the modified parameters [Eqs. (6)]. As is seen in this figure, for low frequencies $\omega<300$ cm^{-1} the density calculated for the two models almost coincides while for high frequencies $\omega>1000$ cm^{-1} substantial differences can be noticed. In fact, the use of the Brenner potential moves the high-frequency edge of the spectrum to the right by at least 100 cm^{-1}; the latter contradicts the experimental data for the upper cutoff frequency $\omega_m\approx 1600$ cm^{-1}. Moreover, the high-frequency region of the spectrum appears to be substantially narrowed. Therefore, in what follows we will use mainly the molecular-dynamics potential [Eq. (8)] which we believe describes the frequency spectrum more adequately.

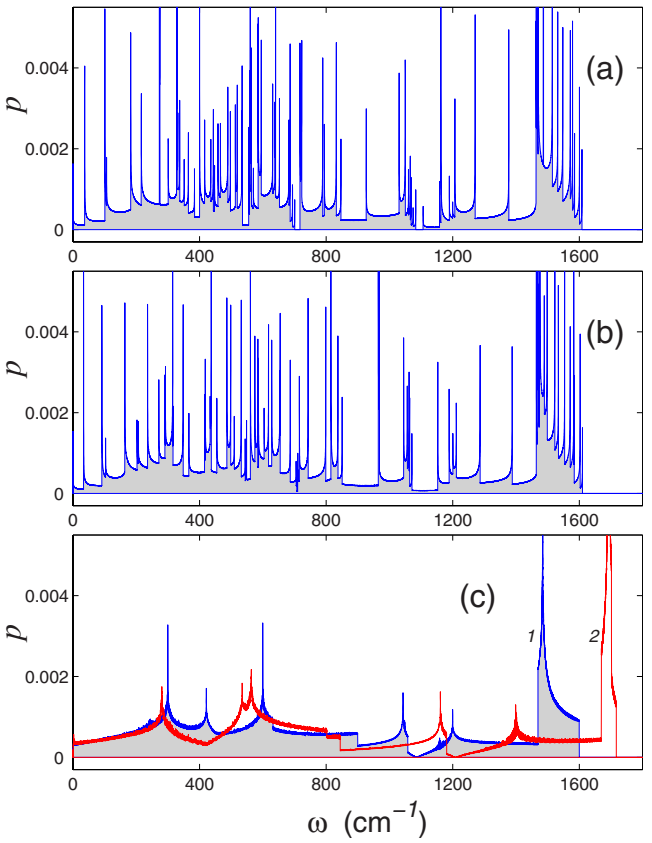

FIG. 4. (Color online) Density of states $p(\omega)$ for small-amplitude oscillations of a carbon nanotube with the chirality indices (a) (10,0), (b) (6,6), and (c) (600,600) obtained for the model with the molecular-dynamics potential [Eq. (8)]. For comparison, the case (c) also shows the results obtained with the use of the Brenner potential with the parameters [Eqs. (6)] (curve 1 corresponds to the standard potential and curve 2 corresponds to the Brenner potential). The density of states is normalized by the condition $\int_0^\infty p(\omega)d\omega=1$.

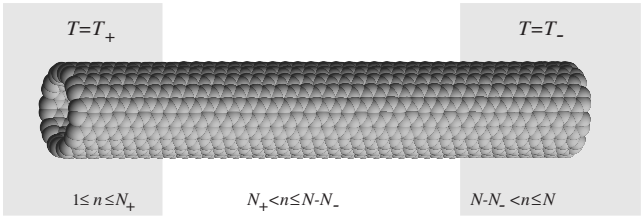

FIG. 5. Example of the nanotube (10,10) with N longitudinal steps. First left N_+ segments are attached to the $T=T_+$ thermostat and the last right N_- segments are attached to the $T=T_-$ thermostat.

IV. NUMERICAL METHODS FOR ANALYZING THE THERMAL CONDUCTIVITY

For numerical modeling of the heat transfer along the nanotube, we consider a nanotube of a fixed length with the edges placed in the thermostats of different temperatures, as shown in Fig. 5. For calculating the coefficient of thermal conductivity, we should be able to calculate numerically the heat flux through any cross section of the nanotube. Therefore, first we need to obtain a formula for a longitudinal local heat flux.

First, we consider the nanotube with the chirality index $(m,0)$. If the six-dimensional vector $\mathbf{x}_{n,l}=(x_{n,l,0},y_{n,l,0},z_{n,l,0},x_{n,l,1},y_{n,l,1},z_{n,l,1})$ defines the coordinates of atoms in the elementary cell (n,l), we can present the system Hamiltonian in the form

$$H=\sum_n \sum_{l=0}^{m-1}\left[\frac{1}{2}M\dot{\mathbf{x}}_{n,l}^2+P(\mathbf{x}_{n-1,l},\mathbf{x}_{n,l-1},\mathbf{x}_{n,l},\mathbf{x}_{n,l+1},\mathbf{x}_{n+1,l})\right], \tag{20}$$

where the first term describes the kinetic energy of atoms in the cell and the second term describes the energy of interaction between the atoms and with the atoms of the neighboring cells. The motion equations following Hamiltonian (20) can be written in the form

$$\begin{aligned}M\ddot{\mathbf{x}}_{n,l}=&-P_1(\mathbf{x}_{n,l},\mathbf{x}_{n+1,l-1},\mathbf{x}_{n+1,l},\mathbf{x}_{n+1,l+1},\mathbf{x}_{n+2,l})\\&-P_2(\mathbf{x}_{n-1,l+1},\mathbf{x}_{n,l},\mathbf{x}_{n,l+1},\mathbf{x}_{n,l+2},\mathbf{x}_{n+1,l+1})\\&-P_3(\mathbf{x}_{n-1,l},\mathbf{x}_{n,l-1},\mathbf{x}_{n,l},\mathbf{x}_{n,l+1},\mathbf{x}_{n+1,l})\\&-P_4(\mathbf{x}_{n-1,l-1},\mathbf{x}_{n,l-2},\mathbf{x}_{n,l-1},\mathbf{x}_{n,l},\mathbf{x}_{n+1,l-1})\\&-P_5(\mathbf{x}_{n-2,l},\mathbf{x}_{n-1,l-1},\mathbf{x}_{n-1,l},\mathbf{x}_{n-1,l+1},\mathbf{x}_{n,l}),\end{aligned} \tag{21}$$

where the function P_j is defined as

$$P_j=\frac{\partial}{\partial\mathbf{x}_j}P(\mathbf{x}_1,\mathbf{x}_2,\mathbf{x}_3,\mathbf{x}_4,\mathbf{x}_5),\quad j=1,2,\ldots,5.$$

To determine the energy flux through the nanotube cross section, we present formula (20) in a compact form, $H=\Sigma_n h_n$, where h_n is the energy density,

$$h_n=\sum_{l=0}^{m-1}\left[\frac{1}{2}M\dot{\mathbf{x}}_{n,l}^2+P(\mathbf{x}_{n-1,l},\mathbf{x}_{n,l-1},\mathbf{x}_{n,l},\mathbf{x}_{n,l+1},\mathbf{x}_{n+1,l})\right]. \tag{22}$$

Local longitudinal heat flux j_n is defined through the local energy density h_n by the discrete version of the continuity equation,

$$\frac{d}{dt}h_n=j_n-j_{n+1}. \tag{23}$$

Using the energy density [Eq. (22)] and the motion equations [Eq. (21)], we can derive the following relations:

$$\begin{aligned}\frac{d}{dt}h_n=&\sum_{l=0}^{m-1}[M\dot{\mathbf{x}}_{n,l}\ddot{\mathbf{x}}_{n,l}+P_{1,n,l}\dot{\mathbf{x}}_{n-1,l}+P_{2,n,l}\dot{\mathbf{x}}_{n,l-1}+P_{3,n,l}\dot{\mathbf{x}}_{n,l}\\&+P_{4,n,l}\dot{\mathbf{x}}_{n,l+1}+P_{5,n,l}\dot{\mathbf{x}}_{n+1,l}]=\sum_{l=0}^{m-1}[-P_{1,n+1,l}\dot{\mathbf{x}}_{n,l}\\&-P_{5,n-1,l}\dot{\mathbf{x}}_{n,l}+P_{1,n,l}\dot{\mathbf{x}}_{n-1,l}+P_{5,n,l}\dot{\mathbf{x}}_{n+1,l}],\end{aligned}$$

where

$$P_{j,n,l}=P_j(\mathbf{x}_{n-1,l},\mathbf{x}_{n,l-1},\mathbf{x}_{n,l},\mathbf{x}_{n,l+1},\mathbf{x}_{n+1,l}),$$

$j=1,2,\ldots,5$. From this and Eq. (23) it follows that the energy flux through nth cross section has the following simple form:

$$j_n=\sum_{l=0}^{m-1}[P_{1,n,l}\dot{\mathbf{x}}_{n-1,l}-P_{5,n-1,l}\dot{\mathbf{x}}_{n,l}].$$

For the nanotube with the chirality index (m,m), Hamiltonian takes the form $H=\Sigma_n h_n$, with the local energy density

$$h_n=\sum_{l=0}^{m-1}\left[\frac{1}{2}M\dot{\mathbf{x}}_{n,l}^2+P(\mathbf{x}_{n-1,l},\mathbf{x}_{n,l+1},\mathbf{x}_{n,l},\mathbf{x}_{n,l-1},\mathbf{x}_{n+1,l})\right].$$

Here j_n is the energy flux through the nth cross section of the nanotube,

$$j_n=\sum_{l=0}^{m-1}[(P_{1,n,l}+P_{2,n,l-1})\dot{\mathbf{x}}_{n-1,l}-(P_{4,n-1,l+1}+P_{5,n-1,l})\dot{\mathbf{x}}_{n,l}].$$

For a direct numerical modeling of the heat transfer along the carbon nanotube, we consider a finite structure of the length $N\Delta h$ with fixed ends. We assume that the first $N_+=40$ segments are placed in the thermostat $T_+=310$ K and the last $N_-=40$ segments are placed in the other thermostat at $T_-=290$ K. The nanotube dynamics is described by the following equations of motion:

$$\begin{aligned}&M\ddot{\mathbf{x}}_{n,l}=-\mathbf{F}_{n,l}-\Gamma M\dot{\mathbf{x}}_{n,l}+\Xi_{n,l}^+,\\&n=2,\ldots,N_+,\\&M\ddot{\mathbf{x}}_{n,l}=-\mathbf{F}_{n,l},\\&n=N_++1,\ldots,N-N_-,\\&M\ddot{\mathbf{x}}_{n,l}=-\mathbf{F}_{n,l}-\Gamma M\dot{\mathbf{x}}_{n,l}+\Xi_{n,l}^-,\\&n=N-N_-+1,\ldots,N,\end{aligned} \tag{24}$$

where $F_{n,l}=\partial H/\partial\mathbf{x}_{n,l}$, $l=0,\ldots,m-1$, $\Gamma=1/t_r$ is the damping coefficient (relaxation time $t_r=0.1$ ps), and $\Xi_{n,l}^{\pm}$

$=(\xi^{\pm}_{n,l,1},\ldots,\xi^{\pm}_{n,l,6})$ is six-dimensional vector of normally distributed random forces normalized by the condition

$$\langle \xi^{\pm}_{n,k,i}(t_1)\xi^{\pm}_{m,l,j}(t_2)\rangle = 2Mk_B\Gamma T_{\pm}\delta_{nm}\delta_{kl}\delta_{ij}\delta(t_1-t_2).$$

We take the initial conditions corresponding to the equilibrium state of the nanotube,

$$\{\mathbf{x}_{n,l}(0)=\mathbf{x}^0_{n,l},\ \dot{\mathbf{x}}_{n,l}(0)=\mathbf{0}\}^{N,m-1}_{n=1,l=0}, \tag{25}$$

where the equilibrium coordinates of atoms $\mathbf{x}^0_{n,l}$ are defined by Eqs. (1), for the nanotube $(m,0)$, and by Eqs. (2), for the nanotube (m,m). With these initial conditions, we intergrade numerically the equations of motion [Eqs. (24)] by employing the Verlet velocity method with the step $\Delta t=0.0005$ ps. After some integration time t_0 [this value depends on the nanotube length between the thermostats, $\Delta L=(N-N_+-N_-)\Delta h$], we observed the formation of a temperature gradient and a constant heat energy flux in the central part of the nanotube. The time t_0 for approaching this stationary regime grows with the nanotube length. For $N=90$ ($\Delta L=10\Delta h=2.17$ nm), it is sufficient to take $t_0=10$ ps, but for $N=2640$ (length $\Delta L=555.5$ nm), the stationary regime is reached only after $t=800$ ps. It is important to notice that the time t_0 can be reduced by modifying the initial distribution of the energy, e.g., taking the initial condition for the system [Eqs. (24)] as homogeneously thermalized state with the mean temperature $T=(T_++T_-)/2=300$ K.

After the stationary heat flux is established, we can find the temperature distribution by using the formula

$$T_n=\lim_{t\to\infty}\frac{M}{6mk_Bt}\int_0^t\sum_{l=0}^{m-1}\dot{\mathbf{x}}^2_{n,l}(\tau)d\tau$$

and the averaged value of the energy flux along the nanotube

$$J_n=\lim_{t\to\infty}\frac{\Delta h}{t}\int_0^t j_n(\tau)d\tau. \tag{26}$$

Distributions of the local energy flux and temperature along the nanotube are shown in Figs. 6(a) and 6(b). In the steady-state regime, the heat flux through each of the cross section at the central part of the nanotube should remain the same, i.e., $J_n\equiv J$, $N_+<n\le N-N_-$. This property can be employed as a criterion for the accuracy of numerical modeling and can also be used to determine the characteristic time for achieving the steady-state regime and calculation of J_n and T_n. Figure 6(a) suggests that the flux is constant along the central part of the nanotube thus suggesting we achieved the required regime.

At the central part of the nanotube, we observe the linear gradient of the temperature distribution, so that we can define the coefficient of thermal conductivity as

$$\kappa(N-N_+-N_-)=\frac{(N-N_--N_+-1)J}{(T_{N_++1}-T_{N-N_-})S}, \tag{27}$$

where $S=\pi R^2$ is the area of the cross section of the nanotube (R is the radius). The result [Eq. (27)] can be improved further provided we approximate the temperature in the central part of the nanotube by a linear function, $T_n\approx\alpha n+\beta$. Then, formula (27) becomes $\kappa(N-N_+-N_-)=J/S\alpha$. In this way, the calculation of thermal conductivity is reduced to the calculation of the limiting value,

$$\kappa=\lim_{N\to\infty}\kappa(N). \tag{28}$$

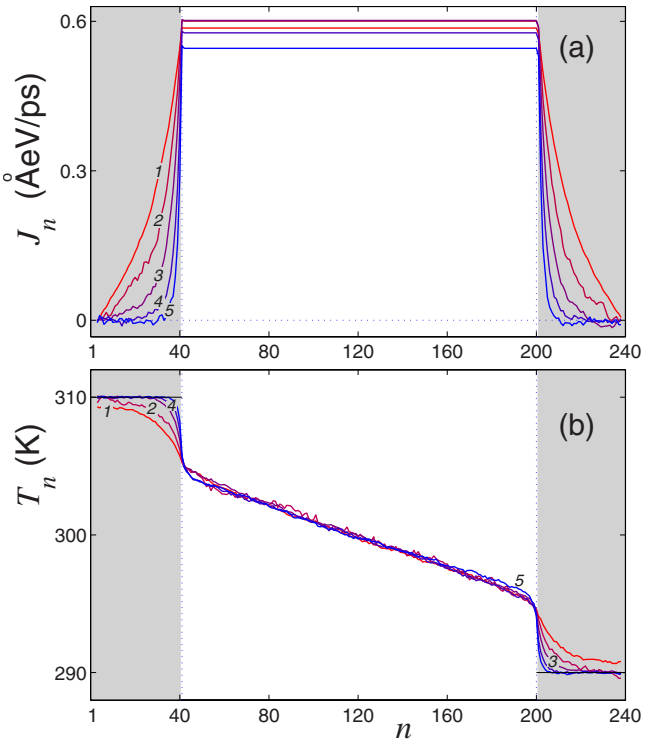

FIG. 6. (Color online) Distributions of (a) local heat flux J_n and (b) local temperature T_n in the nanotube (6,6) for relaxation times $t_r=0.4$, 0.2, 0.1, 0.05, and 0.025 ps (curves 1–5). The parameters are length $N\Delta h=29.52$ nm ($N=240$, $\Delta h=0.123$ nm), temperatures $T_+=310$ K and $T_-=290$ K, and the number of cells in the thermostats, $N_\pm=40$. The averaging time is $t=1$ ns. The regions placed in the thermostats are shown in gray, $1<n\le N_+$, $N-N_-<n\le N$.

It is important to mention that the linear distribution of temperature in the central part of the nanotube and the value of the thermal flux depend only weakly on the relaxation time of atoms t_r at the hot and cold edges [see Fig. 6(b)]. More substantial changes are observed for relatively large viscosity of thermostat, $t_r=0.025$ ps. Here a small decrease of the flux is compensated by a change of the temperature gradient inside the nanotube, so that the resulting value of the thermal conductivity coefficient remains almost unchanged. For example, for the nanotube with chirality (6,6) and $N=240$ elements the coefficient of thermal conductivity $\kappa(N-N_+-N_-)=380-390$ W/mK for $t_r=0.025$, 0.05, 0.1, 0.2, and 0.4 ps. In what follows, we use the fixed value $t_r=0.1$ ps that corresponds approximately to the relaxation time of a single atomic oscillation in a nonthermalized nanotube, i.e., the time when the energy decays in e times due to the radiation of phonons.

In order to determine the coefficient of thermal conductivity, we need to know only the dependence of the temperature in the central part of the nanotube. However, a change of

the temperature distribution at the edges of the nanotube can also provide some useful information. If the nanotube is placed into a Langevin thermostat at temperature T, each segment of the nanotube should have the temperature $T_n=T$ due to the energy balance of the input energy from random forces and the energy lost to dissipation. Then, an averaged energy flow from the nth segment of the nanotube can be presented as

$$\Gamma M \sum_{l=0}^{m-1} \langle \dot{\mathbf{x}}_{n,l}^2 \rangle = 6mk_B T_n / t_r.$$

If only the edges of the nanotube are placed into thermostat, there appears an additional energy exchange with its central part, so the energy from the right edge will flow to the left edge. As a result, the temperature of the left edge is reduced ($T_n \leq T_+$), whereas the temperature at the right edge grows ($T_n \geq T_-$) (see Fig. 6). This information allows us to find the energy flux in the central part of the nanotube using only the energy imbalance at the edges,

$$\frac{Jt_r}{\Delta h 6mk_B} = \sum_{n=1}^{N_+} (T_+ - T_n) = \sum_{n=N-N_-+1}^{N} (T_n - T_-). \quad (29)$$

If the lengths of the edges placed into thermostat coincide, i.e., $N_+=N_-=N_\pm$, we can rewrite this formula in the following simplified form:

$$J = \frac{\Delta h 3mk_B}{t_r} \sum_{n=1}^{N_\pm} (T_+ - T_- - T_n + T_{N+1-n}).$$

Equation (29) gives an alternative way for calculating the thermal energy flux J and can be employed for verifying the results obtained with the help of Eq. (26). Our numerical simulations demonstrate that both these formulas lead to the same value of the thermal energy flux, J.

Another method for the study of thermal conductivity coefficient κ is connected with the Green-Kubo formula,[50]

$$\kappa = \frac{1}{k_B T^2} \lim_{t\to\infty} \int_0^t \lim_{N\to\infty} \frac{1}{V} \langle \mathbf{J}(s) \cdot \mathbf{J}(0) \rangle ds, \quad (30)$$

where $V=\pi \Delta h R^2 N$ is the volume of the nanotube of the length $N\Delta h$ and $\mathbf{J}$ is the total energy flux,

$$\mathbf{J} = \Delta h \sum_{n=1}^{N} j_n,$$

along a finite nanotube with the periodic boundary conditions. Formula (30) can be written in the form

$$\kappa = \frac{1}{k_B T^2 \pi R^2 \Delta h} \lim_{t\to\infty} \int_0^t C(s) ds, \quad (31)$$

where we introduce the heat flux autocorrelation function

$$C(t) = \lim_{N\to\infty} \frac{1}{N} \langle \mathbf{J}(t) \cdot \mathbf{J}(0) \rangle, \quad (32)$$

and the averaging $\langle \cdot \rangle$ should be made for all thermalized states of the nanotube.

In this second approach for calculating the thermal conductivity coefficient we need to calculate the integral [Eq. (31)]. If this integral diverges, then the nanotube has an infinite thermal conductivity. Numerically, the correlation function [Eq. (32)] can be calculated for a finite chain as follows:

$$C_N(t) = \frac{1}{N} \langle \mathbf{J}(s) \cdot \mathbf{J}(s-t) \rangle_s. \quad (33)$$

Here, we need to take a large enough number of cells N for a better convergence of the approximated function $C_N(t)$ to the correlation function $C(t)$. Our numerical results demonstrate that it is necessary to take $N=2000$ for the nanotube with the chirality $(m,0)$, but the nanotube with the chirality (m,m) requires the value $N=3000$. In connection with this we notice that the value $N=64$ used in one of the earlier studies[27] seems insufficient, and the correlation function for such short steps looks like a noise which carries no useful information.

To find the correlation function we need to solve numerically a finite system of equations of motion [Eq. (21)], $n=1,2,\ldots,N$, with the periodic boundary conditions and the initial conditions corresponding to a thermalized state of the nanotube. For this purpose, we employ the Langevin equations,

$$M\ddot{\mathbf{x}}_{n,l} = -\mathbf{F}_{n,l} - \Gamma M \dot{\mathbf{x}}_{n,l} + \Xi_{n,l},$$

$$n = 1,2,\ldots,N, \quad l = 0,1,\ldots,m-1, \quad (34)$$

where the function $F_{n,l}$ is defined by expression (16), $\Gamma = 1/t_r$ is the damping coefficient, t_r is the relaxation time of the atom (we can use here the value $t_r=0.1$ ps), and $\Xi_{n,l} = (\xi_{n,l,1},\ldots,\xi_{n,l,6})$ is the six-dimensional vector of normally distributed random forces describing the interaction of atoms of the cell (n,l) with the thermostat. The random forces are assume to have the standard correlation properties,

$$\langle \xi_{n,k,i}(t_1) \xi_{m,l,j}(t_2) \rangle = 2M\Gamma k_B T \delta_{nm} \delta_{kl} \delta_{ij} \delta(t_1 - t_2), \quad (35)$$

where k_B is the Boltzmann constant and T is the thermostat temperature.

In order to achieve a thermalize state, we integrate the Langevin system [Eqs. (34)] with the initial conditions [Eq. (25)] corresponding to the equilibrium state of the nanotube for the period of time $t=20t_r$. To increase the accuracy of the numerical calculations, we make the averaging in Eq. (33) for 10^3 independent realizations of the thermalized nanotube.

The form of the correlation function $C(t)$ depends substantially on the nanotube chirality (see Fig. 7). For example, for the nanotube with the chirality index (m,m) this function does not have any high-frequency oscillations, after about 0.4 ps all oscillations decay rapidly, and then the function tends to zero monotonously for $t\to\infty$ [see Fig. 7(a)]. For the nanotube with the chirality index $(m,0)$, we observe always high-frequency oscillations for $t<3$ ps. However, these oscillations decay for longer time and the function becomes monotonically decaying for $t\to\infty$ [see Figs. 7(b) and 7(c)]. We observe that the oscillation amplitude grows sharply and decays slowly in the case of the use of the Brenner potential

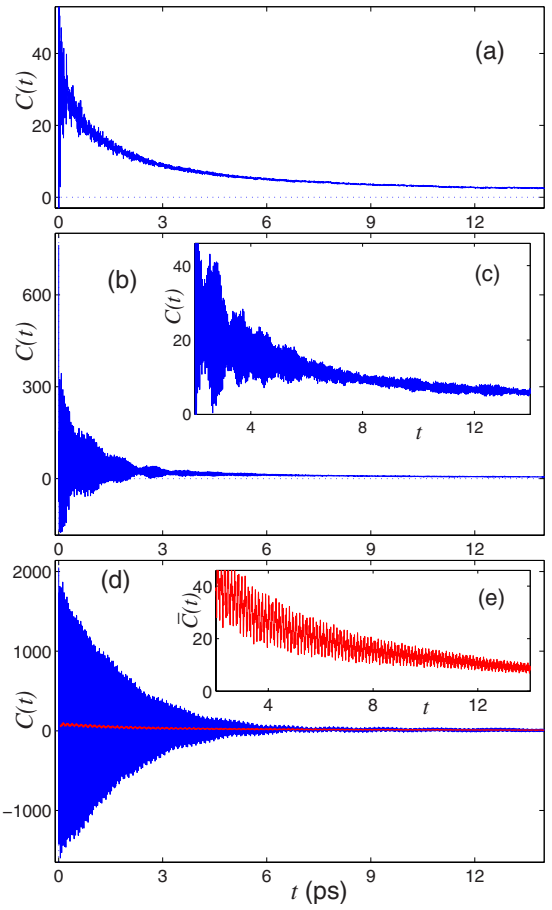

FIG. 7. (Color online) Correlation function $C(t)$ (in the units $[C]=(\text{eV Å/ps})^2$) for $T=300$ K and (a) nanotube (6,6) and (b) and (c) nanotube (10,0) calculated with the use of the molecular-dynamics potentials [Eq. (8)]. For comparison, in (d) and (e) we show the correlation function for the nanotube (10,0) obtained for the Brenner potential [red (gray) curve shows a smoothen dependence]. In calculations, we used $N=3000$ periods for the nanotube (6,6) and $N=2000$ periods for the nanotube (10,0).

[see Fig. 7(d)]. In this case, we may estimate the correlation function only if we consider the smoothen dependence calculated as

$$\bar{C}(t) = \frac{1}{\Delta t}\int_{t-\Delta/2}^{t+\Delta/2} C(s)ds,$$

which provides averaging of high-frequency oscillations for $\Delta t=0.1$ ps. This smoothen function is shown in Fig. 7(d) in red (gray), and it vanishes rapidly.

We would like to mention that the high-frequency oscillations of the heat flux autocorrelation function are not related with the averaging procedure. They appear for any number of independent realizations of thermalized states of the nanotube. To understand the origin of these oscillations, we find their frequency spectrum and compare it with the frequency spectrum of small-amplitude oscillations of the nanotube itself. When we use the molecular-dynamics potential, for the nanotube (10,0) we observe the oscillations of the correlation function with the main frequency ω $=847$ cm^{-1}, as shown in Fig. 8. This frequency coincides with the frequency $\omega_{0,4}(0)$ of the radial optical oscillations [see Fig. 3(a)]. In the vicinity of this frequency there are three dispersion curves with a weak dependence on the wave number q. For the nanotube (6,6), this frequency corresponds to a single mode that decays more rapidly with q [see Fig. 3(d)]. Therefore, the radial optical oscillations of the nanotube (6,6) will decay faster than those for the nanotube (10,0). As a result, the oscillations of the correlation function for the nanotube (6,6) decay much faster.

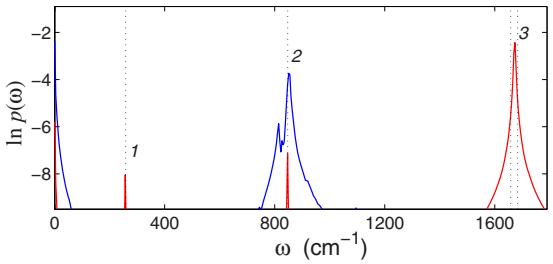

FIG. 8. (Color online) Density of states $p(\omega)$ for decaying oscillations of the correlation function $C(t)$ for the nanotube (10,0) calculated for the molecular-dynamics potential [Eq. (8)] (blue) and the Brenner potential [red (gray) curve]. The first peak corresponds to the frequency of 258 cm^{-1}, second −847 cm^{-1}, and the third −1670 cm^{-1}. The density is normalized by the condition $\int_0^\infty p(\omega)d\omega=1$.

The frequency spectrum of the correlation function calculated with the help of the Brenner potential displays three peaks, as shown in Fig. 8. The main peak at the frequency of 1670 cm^{-1} corresponds to the optical torsion oscillations of the nanotube. Since these oscillations are not described well by the Brenner potential, the obtained spectrum appears as being very narrow [1658,1683] cm^{-1} and the dispersion curves do not depend on the wave number [see Fig. 3(c)]. Therefore, such oscillation will decay very slow giving rise to high-frequency oscillations of the correlation function. The second peak corresponds to radial optical oscillations with the frequency $\omega_{0,4}(0)=847$ cm^{-1} and the third peak corresponds to radial acoustic oscillations with the frequency $\omega_{0,3}(0)=257$ cm^{-1}.

V. THERMAL CONDUCTIVITY: A SUMMARY OF RESULTS

Our studies demonstrate that thermal conductivity of the nanotube depends dramatically on its interaction with a substrate. More specifically, an isolated nanotube demonstrates anomalous (infinite) conductivity, whereas a nanotube placed on a flat substrate changes its conductivity to normal (finite) one. Therefore, below we consider these two cases separately.

A. Isolated nanotubes

Our extensive numerical results demonstrated that the heat flux autocorrelation function of an isolated nanotube always decays in accord with the power-law dependence

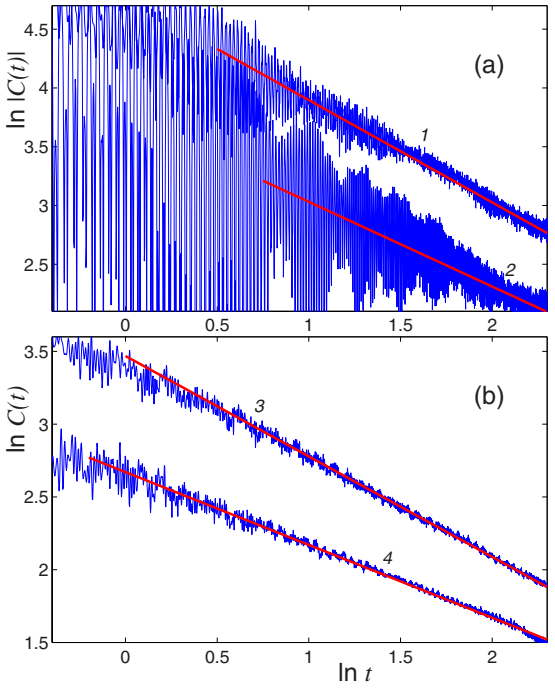

FIG. 9. (Color online) Power-law decay of the heat flux autocorrelation function $C(t)$ for (a) nanotubes (20,0) and (10,0) (curves 1 and 2) and (b) nanotubes (6,6) and (3,3) (curves 3 and 4) (dimensions are $[t]$=ps and $[C]$=(eV Å/ps)^2). Straight lines define the dependence $t^{-\alpha}$ with exponents α=0.87, 0.72, 0.69, and 0.5 (lines 1–4). Temperature T=300 K.

$$C(t) \sim t^{-\alpha} \quad \text{when} \quad t \to \infty, \tag{36}$$

with the exponent α growing monotonically with the nanotube radius but remaining always $\alpha < 1$ (see Fig. 9). For the nanotubes with the chirality indices (3,3) and (5,0), the exponent is α=0.5, for the nanotubes (6,6) and (10,0), it is α =0.7, and for the nanotube (20,0), we find α=0.9. It is important to mention that we have verified that the use of the Brenner potential gives the same values of α, but it requires to smoothen the correlation function $\bar{C}(t)$.

From the asymptotic dependence [Eq. (36)] it follows the divergence of the integral in Green-Kubo formula (31) and therefore the infinite thermal conductivity of an isolated nanotube. The divergence rate grows monotonically with the decrease of the nanotube radius, so the nanotubes of smaller radius demonstrate more pronounced anomalous conductivity. We confirm these results by a direct modeling of the heat transfer in the nanotube.

Dependence of the coefficient κ on the length L of the nanotube (defined as the length of the part between the two thermostats) is shown in Fig. 10. As follows from this figure, thermal conductivity grows with the length L in accord with the power law, L^β, where growth rate depends on the nanotube radius R but not on its chirality. Figure 10 also shows that for the nanotubes of different chiralities but approximately same radii, e.g., the nanotubes (3,3) and (5,0) (radius R=2 Å) and (6,6) and (10,0) (radius R=4 Å), thermal conductivity grows with the same rates, β=0.38 for R=2 Å and β=0.21 for R=4 Å. For large enough L the nanotubes with

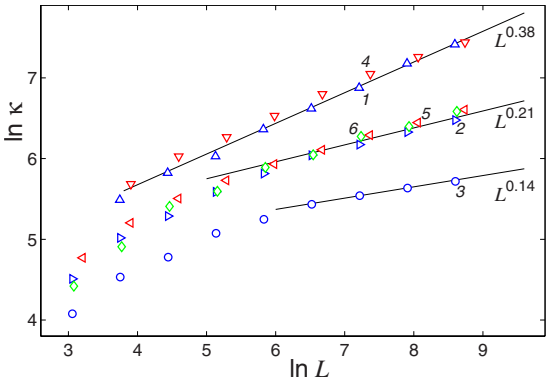

FIG. 10. (Color online) Dependence of the coefficient of thermal conductivity κ on the length of the central part of the nanotube, L. Dimensions are $[\kappa]$=W/mK and $[L]$=Å. Markers 1–5 correspond to nanotubes (5,0), (10,0), (20,0), (3,3), and (6,6), respectively. Three lines show the dependencies $\kappa \sim L^\beta$ with β=0.38, 0.21, and 0.14. Marker 6 shows the dependence $\kappa/1.3$ for nanotube (10,0) calculated with the help of the Brenner potential.

the same radius have the same thermal conductivity.

Our numerical simulations of the heat transport in isolated nanotubes do confirm the earlier results about infinite thermal conductivity of SWCNTs. The coefficient of thermal conductivity κ of the nanotube of a fixed length L depends only on its radius R, and $\kappa(L)$ decreases with the radius. This dependence seems obvious because in the definition [Eq. (27)] the heat flow J is divided by the area of the nanotube cross section, $S=\pi R^2$. Since the number of particles in the cross section is proportional to the circumference $2\pi R$, but not the area, we obtain $\kappa \to 0$ for $R \to \infty$. For such a definition, the thermal conductivity coefficient κ of a graphite sheet will tend to zero. To avoid this dimension effect, we use the renormalized coefficient, $\kappa_c = \kappa R/2$, when the energy flow through the cross section is divided by the circumference but not the area.

Dependence of the renormalized coefficient of thermal conductivity κ_c on the length of the nanotube length L is shown in Fig. 11. As follows from this figure, the thermal conductivity grows with R even after the normalization, but the growth rate decreases for larger nanotube radii. For example, for R=2 Å [nanotube (5,0)], we have β=0.38, for R=4 Å [nanotube (10,0)], we have β=0.21, and for R =8 Å [nanotube (20,0)], we obtain β=0.14. Thus, the anomalous conductivity will manifest itself more strongly for the nanotubes of smaller radius.

We notice that for large values of the nanotube radius R we should expect a substantially different dependence of the normalized coefficient κ_c because it is known that for $R \geq 11$ Å SWCNTs become bistable and create a new fully collapsed state (the nanotube changes its three-dimensional structure to a flat two-layer stripe), and for $R > 30$ Å only this collapsed state will remain stable.[51–53] It is expected that such a dramatic change of the nanotube geometry will modify substantially the nanotube properties including its thermal conductivity. However, this problem is beyond the scope of our study where we always assume the nanotubes of smaller radii.

Thermal conductivity of a long multiwall nanotube also decays monotonically with its radius. The similar behavior

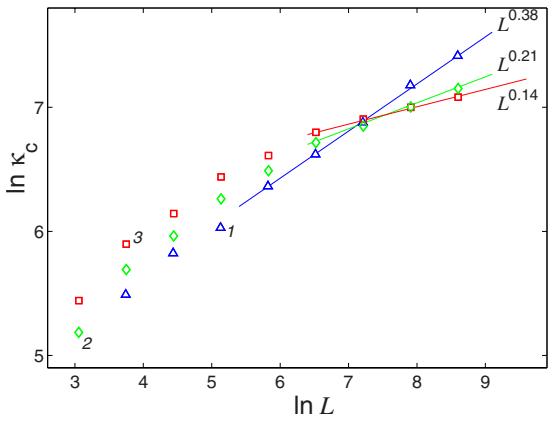

FIG. 11. (Color online) Dependence of the renormalized coefficient of thermal conductivity κ_c on the length of the central part of the nanotube L. Dimensions are $[\kappa_c]=W\times 10^{-10}/\mathrm{K}$ and $[L]=\text{Å}$. Markers 1–3 to the nanotubes (5,0), (10,0), (20,0), respectively. Three lines show the dependencies $\kappa_c \sim L^{\beta}$ with $\beta=0.38$, 0.21, and 0.14.

was observed experimentally.[11] Indeed, the experimental data suggest that for room temperature thermal conductivity grows with a decrease of the nanotube radius and reach the value of 2000 W/mK for the diameter of 9.8 nm (for the nanotube length $L=3.70$ μm).

We notice that the use of the Brenner potential gives the same values of the exponents α and β, but for large L the obtained values of the thermal conductivity coefficient are larger by about 30% (see Fig. 10). This can be explained by an extra "hardness" of the Brenner potential. Similarly, the speed of long-wave torsion and longitudinal acoustic phonons is also larger for the Brenner potential in comparison with the model using the molecular-dynamics potentials (see Tables I and II). This suggests, once more, that the character of thermal conductivity is defined by the main contribution from long-wave acoustic phonons which define the ballistic energy flow being responsible for the overall infinite thermal conductivity. In a sharp difference, the study of the nanotube interacting with a substrate gives completely different results, as shown in Sec. V B.

B. Nanotubes interacting with a substrate

Now we study the effect of substrate on thermal conductivity of a nanotube. We consider the nanotube placed on a flat crystalline surface (e.g., a surface of a Si crystal). For simplicity, we assume that only nearest neighbors interact (see Fig. 12). As the first approximation, we assume that the substrate atoms do not move. Then, the thermal energy exchange is absent, and the interaction can be described by an additional on-site potential $U(x,y,z)=K_0(x^2+y^2+z^2)/2$, where (x,y,z) is the displacement of the atom from its equilibrium position and K_0 is the elasticity coefficient. For the valent interaction between the atoms, $K_0 \approx 300$ N/m, whereas for nonvalent interaction, $K_0 \approx 3$ N/m. We add the on-site potential U into Hamiltonians (3) and (20) only for the atoms interacting with the substrate and make the corresponding changes in the motion equations [Eqs. (15), (21), and (24)]. Importantly, the formulas defining the local heat flux j_n will not change, and we may apply the same methods as used above for the isolated nanotube, including the equilibrium dynamics based on the Green-Kubo formula.

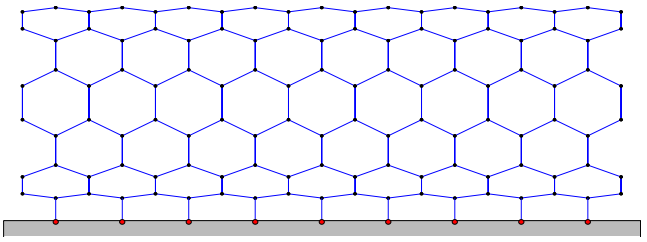

FIG. 12. (Color online) Schematic of a (6,6) nanotube interacting with the atoms of the substrate.

Interaction with the substrate leads to the disappearance of long-wave acoustic phonons and appearance of a narrow gap $[0,\omega_0]$ at the bottom of the frequency spectrum of small-amplitude oscillations. For example, for the nanotube (3,3) and $K_0=300$ N/m the gap width is $\omega_0=25$ cm^{-1} and for $K_0=3$ N/m the frequency is $\omega_0=2.5$ cm^{-1}. For numerical modeling, a nanotube of a smaller radius is more convenient to study, so we consider the nanotube (3,3).

The appearance of a gap in the frequency spectrum of small oscillations of the nanotube leads to a dramatic change of the character of its thermal conductivity. For $t\to\infty$ the correlation function $C(t)$ decays faster than the dependence t^{-1} found earlier. For example, for the nanotube (3,3) with hard interaction ($K_0=300$ N/m), the correlation function decays in accord with a power law $t^{-\alpha}$, where $\alpha=1.3>1$ (see Fig. 13). Therefore, we expect that a nanotube interacting with a substrate should have a finite thermal conductivity. We point out to an analogy with the thermal conductivity of one-dimensional nonlinear chains: an isolated Fermi-Pasta-Ulam nonlinear chain is known to have infinite conductivity, which becomes finite in the presence of a substrate potential.[54]

The asymptotic dependence $C(t)\sim t^{-1.3}$ for the nanotube (3,3) allows to find, from Green-Kubo formula (31), the con-

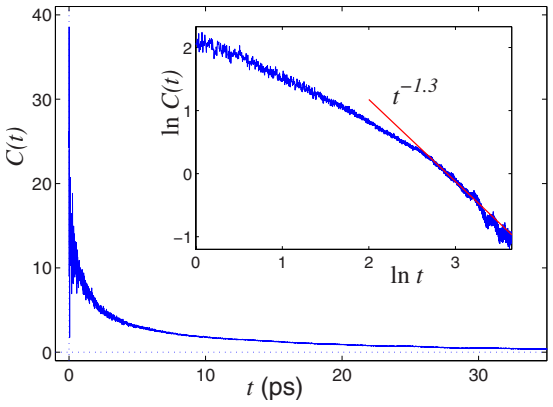

FIG. 13. (Color online) Power-law decay of the heat flux autocorrelation function $C(t)$ of the nanotube on a plane substrate for the chirality index (3,3). Straight lines show dependence $t^{-\alpha}$ for $\alpha=1.3$. Temperature $T=300$ K, stiffness $K_0=300$ N/m, and dimensions are $[t]=\mathrm{ps}$ and $[C]=(\mathrm{eV\ Å/ps})^2$.

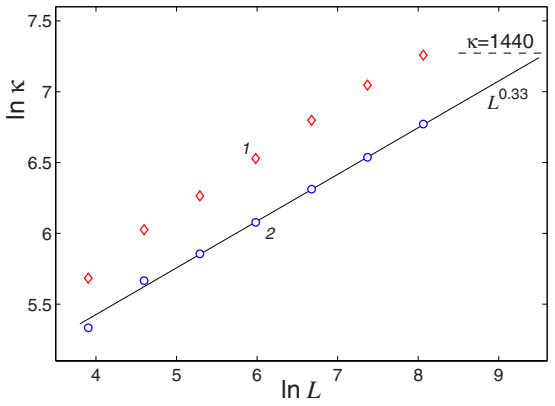

FIG. 14. (Color online) Dependence of the thermal conductivity coefficient κ on the nanotube length L for an isolated nanotube (3,3) (marker 1) and for the nanotube on a plane substrate (marker 2). Temperature $T=300$ K, stiffness $K_0=300$ N/m, and dimensions are $[L]=$Å and $[\kappa]=$W/mK. Line shows dependence $\kappa \sim L^{\beta}$ with $\beta=0.33$.

ductivity coefficient $\kappa=1440$ W/mK. Direct numerical simulations of the heat transfer in the nanotube show that the presence of a substrate changes dramatically the thermal conductivity of a fixed-length nanotube (see Fig. 14). For $L \leq 0.32$ μm, the coefficient $\kappa(L)$ for the nanotube (3,3) grows as a monotonic function $L^{0.33}$. Using the value $\kappa=1440$ W/mK obtained from the Green-Kubo formula, we can evaluate the critical length of the nanotube when the conductivity saturation is observed, $L \sim 1.6$ μm. For weak interaction with the substrate ($K \sim 1$ N/m), the presence of a substrate leads to the appearance of a narrow gap in the frequency spectrum, so that the saturation should be observed for much larger distances. However, the effect of substrate will become even stronger if we take into account the energy exchange between the nanotube and substrate.

In order to take into account the energy exchange between the nanotube and substrate, we should assume that the atoms of the substrate are not fixed, and they can move interacting directly with the thermostat and the substrate atoms. In this case the system "nanotube+substrate" is not closed, and we should only relay on the numerical methods and direct modeling on the thermal conductivity.

We modify the model introducing a coupling between the neighboring atoms, as shown in Fig. 12. If the vector $\mathbf{u}_n=(x_n,y_n,z_n)$ defines the displacement of the substrate atom coupled to the atom (n,l,i) of the nanotube, then the dynamics is described by the following Langevin equations:

$$M\ddot{\mathbf{x}}_{n,l,i} = -\mathbf{F}_{n,l,i} - K_0(\mathbf{x}_{n,l,i} - \mathbf{u}_n),$$

$$M_0\ddot{\mathbf{u}}_n = K_0(\mathbf{x}_{n,l,i} - \mathbf{u}_n) - K_1\mathbf{u}_n - \Gamma M_0\dot{\mathbf{u}}_n + \Theta_n,$$

where the vector $\mathbf{x}_{n,l,i}$ describes the displacement of the nanotube atom with the indices (n,l,i) from its equilibrium position, $F_{n,l,i}=\partial H/\partial \mathbf{x}_{n,l,i}$, the parameter K_0 characterizes the strength of coupling between atoms of nanotube and substrate, M_0 is the mass of the substrate atom, K_1 stands for the interaction between the substrate atoms, $\Gamma=1/t_r$ is the damping coefficient, and $\Theta_n=(\theta_{n,1},\theta_{n,2},\theta_{n,3})$ is the three-dimensional vector of normally distributed random forces with standard correlation properties,

$$\langle \theta_{n,k}(t_1)\theta_{m,l}(t_2)\rangle = 2M_0\Gamma k_B T\delta_{nm}\delta_{kl}\delta(t_1-t_2).$$

Here T is temperature of the substrate. For definiteness, we take $M_0=28m_p$ corresponding to the Si substrate and also select the characteristic value $K_1=300$ N/m and relaxation time $t_r=0.1$ ps.

In our numerical simulations of the thermal conductivity of fixed-length nanotubes, we place the left edge of the nanotube defined as $(1 \leq n \leq N_+)$ into thermostat with temperature $T_+=310$ K and its right edge $(N-N_- < n \leq N)$ into thermostat with temperature $T_-=290$ K. We assume that only the atoms of the central part of the nanotube interact with the substrate, $N_+ < n \leq N-N_-$, where an energy exchange between nanotube and substrate occurs. To avoid additional energy flow from the substrate, we take temperature of the substrate $T=T_-$.

In this case, a nonlinear temperature gradient appears, and the thermal energy flux decays monotonically from the left to right edge (see Fig. 15). Such a behavior is due to the energy exchange between the central part of the nanotube and substrate. A part of the thermal energy is absorbed by the substrate that has temperature $T=T_- < T_+$. Formula (27) remains correct, however we should define correctly the thermal flux

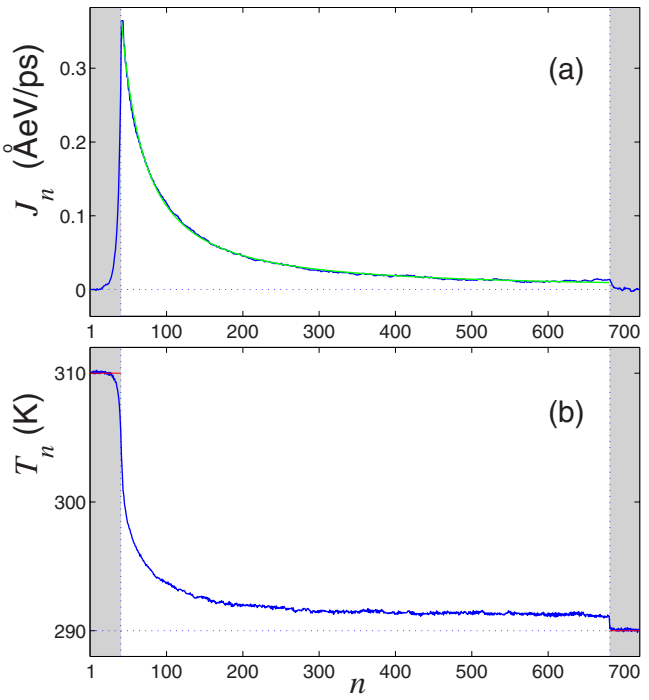

FIG. 15. (Color online) Distribution of (a) local heat flux J_n and (b) local temperature T_n in the nanotube (3,3) in the presence of the energy exchange with a flat substrate (temperature of the left edge $T_+=310$ K, temperature of the right edge $T_-=290$ K, and temperature of the substrate $T=T_-$). The parameters are length $N\Delta h=88.56$ nm ($N=720$, $\Delta h=0.123$ nm), the number of cells in the thermostats, $N_\pm=40$, and interaction potential coefficient $K_0=300$ N/m. The regions placed in the thermostats are shown in gray. Green (light gray) curve in (a) shows the power-law dependence [Eq. (37)] for $\beta=0.025$ and $\alpha=1.30$.

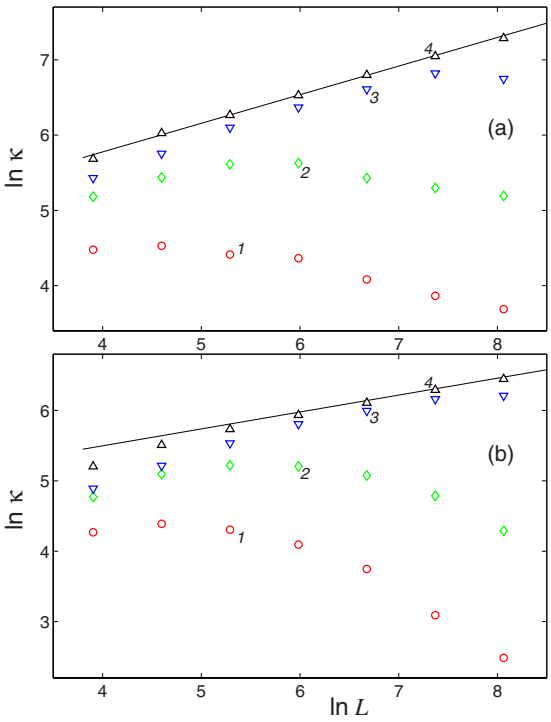

FIG. 16. (Color online) Dependence of the thermal conductivity coefficient κ on the nanotube length L for (a) nanotube (3,3) and (b) nanotube (6,6) interacting with plane substrate for stiffness of interaction $K_0=300$ N/m (marker 1), 30 N/m (marker 2), and 3 N/m (marker 3) and for $K_0=0$ (isolated nanotube, marker 4). Straight lines show the dependences $\kappa \sim L^{0.38}$ and $\kappa \sim L^{0.24}$ for isolate nanotubes. Temperature $T=300$ K; dimensions are $[L]=$Å and $[\kappa]=$W/mK.

J because it varies along the nanotube. To define the thermal flux we need to know the energy transferred between the edges of the nanotube. This energy is defined by the thermal flux near the right edge of the nanotube, therefore we take $J=J_{N-N_-}$.

Our numerical simulations of the heat transfer demonstrate that the energy flux J_n in the central part of the nanotube can be approximated by a power-law function

$$J_n = J_{N_+ +1}/[1+\beta(n-N_+-1)]^{\alpha}, \tag{37}$$

with $\alpha>1$. In particular, for the nanotube (3,3) and valent interaction ($K_0=300$ N/m) we find $\alpha=1.3$ [see Fig. 15(a)]. The power α decreases when the interaction with the substrate becomes weaker but it is always larger than one. For example, for $K_0=30$ we obtain $\alpha=1.14$, and for $K_0=3$ N/m we have $\alpha=1.07$. As a result, the coefficient $\kappa(N)$ will tend to a finite value for $N\to\infty$.

Dependence of the coefficient of thermal conductivity vs the nanotube length is shown in Fig. 16. As follows from those results, due to the interaction with the substrate the thermal coefficient stops to grow. For strong valent coupling between the nanotube and substrate ($K_0=300$ N/m) this occurs for $L\sim 10$ nm, weaker interaction ($K_0=30$ N/m) give a bit longer length, $L\sim 40$ nm, and for very weak nonvalent interaction ($K_0=3$ N/m), we obtain $L\sim 800$ nm. A finite value of the coefficient of thermal conductivity is due to absorption of long-wave phonons by the substrate which in isolated nanotube have infinite propagation length.

Our numerical simulation results demonstrate that all phonons in the nanotube interacting with a substrate have a finite propagation length due to their absorption by the substrate. As a result, the coefficient $\kappa(L)$ decays with the nanotube length L since less phonons reach the right edge of the nanotube. However, this result cannot be extrapolated further, so that we are not able to make a rigorous statement about vanishing thermal conductivity since our modeling does not take into account the thermal energy transferred along the substrate. In reality, more general model describing more complex two-component system nanotube+substrate will show a finite conductivity determined by a thermal conductivity of the substrate and the coupling between the nanotube and substrate. This latter model is close to the system actually measured in experiment. Nevertheless, one of the main conclusions of our study is that such experimental data should not be used for the definition of the thermal conductivity of isolated nanotubes, and the interaction may be crucial changing even the type of the thermal conductivity.

More specifically, our study shows that in the presence of even weak interaction between atoms of nanotube and substrate the thermal conductivity of SWCNT placed on a substrate differs substantially from the conductivity of an isolated nanotube for $L>0.8$ μm. Importantly, the interaction of the nanotube with a substrate not only changes the value of its thermal conductivity $\kappa(L)$ but also modifies the character of this dependence on the length of the nanotube showing saturation for $L\to\infty$. We believe that these results may shed an additional light on a huge variation in the experimental data: 1750–5800 W/mK (see Ref. 3, a crystal of nanotube bunches) and 200 W/mK (Ref. 55, carbon nanotube films).

We notice that the experimental measurement of the length-dependent thermal conductivity of an individual single-walled carbon nanotube is a very difficult problem. The first effort was made in Ref. 38, where authors reported the measurement of the length-dependent thermal conductivities of individual SWCNTs on a Si substrate using a four-pad 3ω method. They observed that, over the length range of 0.7–7 μm, thermal conductivity grows with the length at room temperature. Those authors estimated the phonon free-path length as 180 nm. For SWCNTs longer than this phonon mean path length, dissipative thermal transport is observed, i.e., for larger L the coefficient of thermal conductivity saturates approaching a constant value. Wang *et al.* in Ref. 38 mentioned that such dependence contradicts to the molecular-dynamics simulation results. As a matter of fact, this comparison is not valid because the numerical simulations did not take into account the interaction of the nanotube and substrate. As has been shown above, this interaction is crucial, and it explains a dramatic change of the character of thermal conductivity.

VI. COMPARISON WITH AVAILABLE EXPERIMENTAL DATA

It is important to compare our results for the thermal conductivity $\kappa(L)$ with the experimental data. Measurements of

TABLE III. Experimental data for the thermal conductivity coefficient κ of isolated nanotubes at room temperature. D—external diameter of the nanotube, D_0—internal diameter of multiwall nanotube, and L—the nanotube length.

Ref.		D (nm)	D_0 (nm)	L (μm)	κ (W/mK)
10	MWCNT	14		2.5	3000
11	MWCNT	9.8		3.70	2000
9	SWCNT	2.4		2	3600
12	MWCNT	46	27	1	650–830
13	MWCNT	2		0.7	25000
14	SWCNT	1		2.76	6000
15	SWCNT	1.7		2.6	3500
16	MWCNT	20	10	1.4	300 ± 20
17	MWCNT	10–33		6	290–1050

the thermal conductivity of a single carbon nanotube are extremely difficult, however there exists a number of experimental data already published in the literature,[9–17] which we summarize in Table III. The measured values of κ differ by at least two orders of magnitude, 300–2500 W/mK, which indicate about low accuracy of the methods employed. The nanotube length in the experiments was 0.7–3.7 μm. In numerical simulations, we considered the nanotubes with maximum length $L=0.62$ μm, but we can extrapolate the results to larger values of L in accord with the power law $\kappa(L) \sim L^{\beta}$. The results presented in Table IV do not contradict to those in Table III except one of the value, $\kappa=2.5 \times 10^4$ W/mK, from Ref. 13.

Up to now we considered thermal conductivity at one value of temperature only, $T=300$ K. Now we consider how the thermal conductivity varies with the temperature. Our numerical modeling demonstrates that for all $T \leq 500$ K the heat flux autocorrelation function decays in accord with a power law [Eq. (36)] and only the exponent α varies remaining $\alpha<1$, as shown in Fig. 17. Therefore, the character of the thermal conductivity does not change with temperature.

Energy scattering in the nanotube is associated with nonlinear interatomic interactions. However, the nonlinear oscillations decay monotonically with a decrease of temperature so that for low temperatures the dynamics becomes linear and it can be described as a system of noninteracting linear modes (phonons). Therefore, in the framework of the classical model the thermal conductivity of a finite nanotube should grow indefinitely for $T \to 0$. Our numerical simulations confirm this conjecture. As can be seen in Fig. 18, for any length L the thermal conductivity coefficient $\kappa(L)$ grows monotonically when the temperature decreases, i.e., $\kappa(L) \to \infty$ when $T \to 0$.

This dependence is valid for the classical model when the thermal capacitance does not depend on temperature. In a quantum model the thermal capacitance of the nanotube c decays monotonically with temperature: $c(T) \to 0$ when $T \to 0$. In Refs. 56 and 57 it was shown that thermal capacitance of the nanotube decays linearly with a decrease of temperature. We notice that this result was shown earlier for a thin film,[58] and it is confirmed for the carbon nanotubes in experiment.[59–61] Since the energy carried by a phonon is proportional to its thermal capacitance, the thermal conductivity coefficient should also be proportional to the thermal capacitance. Therefore, the thermal capacitance of the nanotube should tend to zero for $T \to 0$.

In view of our discussions above, it is natural to evaluate the applicability limits of the classical model studied here for the thermal conductivity modeling. Indeed, an oscillatory mode with the frequency ω can be described by a classical model provided $T > T_E$, where $T_E=\omega\hbar/k_B$ is the Einstein temperature. Therefore, the classical model remains valid for $\omega < \omega_E(T)$, where $\omega_E=k_BT/\hbar$. For $T=300$ K we find ω_E

TABLE IV. Extrapolation data for the thermal conductivity coefficient κ (in W/mK) for large length L and different diameters D.

D (nm)	$L=1$ (μm)	$L=2$ (μm)	$L=3$ (μm)	$L=4$ (μm)
0.4	2120	2750	3230	3570
0.8	770	880	960	1022
1.6	340	370	400	410

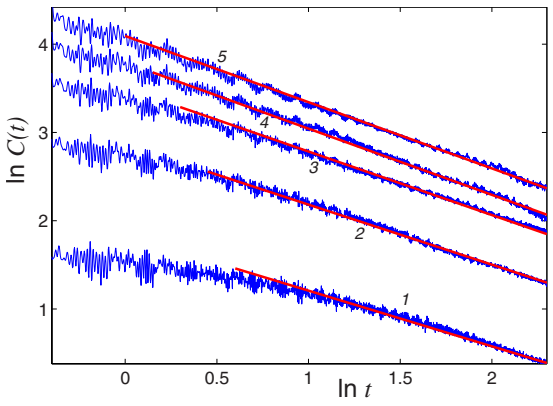

FIG. 17. (Color online) Decay of the correlation function $C(t)$ (in the units of $[C]=(\text{eV Å/ps})^2$ and $[t]=\text{ps}$) for the nanotube (6,6) and temperatures $T=100$, 200, 300, 400, and 500 K (curves 1–5). Straight lines show the power-law dependence $t^{-\alpha}$ with the exponents $\alpha=0.63$, 0.68, 0.72, 0.75, and 0.75.

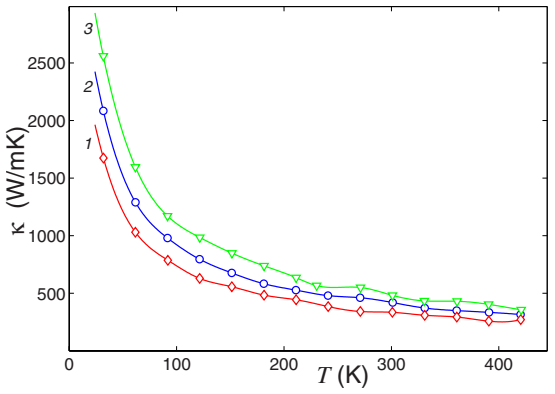

FIG. 18. (Color online) Dependence of the thermal conductivity coefficient κ on temperature T for the nanotube (10,0) and the lengths $L=34$, 68, and 136 nm (curves 1–3, respectively).

$=209\ \mathrm{cm}^{-1}$, so that at room temperature the classical model can describe only low-frequency oscillations of the nanotube. As was shown above, the anomalous thermal conductivity of SWCNT is related with the long-wave (low frequency) acoustic phonons, so the models used here seem adequate, including the case of a nanotube fixed on a substrate.

VII. COMPARISON WITH EARLIER NUMERICAL RESULTS

We believe that it is important to compare our results presented above with many earlier numerical studies of thermal conductivity of isolated single-walled nanotubes.

First of all, we mention that by now, there exist many papers devoted to the numerical modeling of thermal conductivity of carbon nanotubes. All of those studies considered, to the best of our knowledge, only isolated nanotubes, and they all employed the Brenner potential for analyzing the interatomic interaction of carbon atoms in the nanotube. However, as we demonstrated above, the use of the Brenner potential leads to the same results which can be obtained with the help of much simpler molecular-dynamics potentials [Eqs. (7) and (8)]. Therefore, in most of the cases the results do not depend much on the specific type of the potential used but mainly depend on the specific numerical techniques and the properties of the system under consideration.

In the first papers about the numerical modeling of the heat transfer in nanotubes, only very short nanotubes were considered, so that some of the earlier studies led to mistakes. In particular, Berber *et al.*[18] suggested that the SWCNT with the chirality index (10,10) possesses a finite but very large thermal conductivity coefficient ($\kappa=6600$ W/mK). In Ref. 19, for the same nanotube it was found another value, $\kappa=2980$ W/mK, but the modeling was carried out for the length $L=0.04$ μm. The study of short nanotubes (10,10), (11,11), (20,0), and (10,13) carried out in Ref. 23 suggested the dependence of the coefficient κ on the chirality index. Our studies demonstrate that indeed such a dependence is observed for short nanotubes, whereas for larger L thermal conductivity does not depend on the chirality index, but it depends on the nanotube diameter (see Fig. 10). In this limit, the main contribution into thermal conductivity is due to long-wave acoustic phonons which propagate in the nanotube as in an elastic homogeneous cylinder being not sensitive to the discreteness effects. As a result, the nanotubes of different chiralities but similar radius possess the same thermal conductivity. This property has been first mentioned in Ref. 25 where it was also shown the strong dependence of thermal conductivity on temperature and isotopic defects.

The study of thermal conductivity of SWCNT conducted in Ref. 24 was based on the use of the Green-Kubo formula and the method of equilibrium molecular dynamics. It was assumed that thermal conductivity is always finite and that the correlation function $C(t)$ decays exponentially as $\exp(-\lambda t)$. These assumptions were used to calculate the correlation function on a short time interval ($0 \le t \le 3$ ps) and then approximate it for larger t. Our results show that the assumption of the exponential decay of the correlation function is wrong. The similar mistake was made in Ref. 32, where in the study of longer nanotubes (10,0) (with the length $L=5-200$ nm), it was assumed that the integral $\int_0^\infty C_N(t)dt$ converges. Our results presented above show that the main issue here is the convergence of this integral that is determined by the decay rate of the correlation function.

The study of the correlation function conducted in Ref. 26 demonstrated that the thermal conductivity diverges with the growth of the nanotube length. This is indeed confirmed by our analysis for the function $C(t)$ that decays for $t \to \infty$ according to the power law $t^{-\alpha}$ with $\alpha<1$, so that the integral in the Green-Kubo formula (31) diverges.

The first study of the dependence of the thermal conductivity coefficient on the nanotube length has been conducted in Refs. 20 and 22. For the examples of the nanotubes (5,5), (8,8), and (10,10) for the lengths $L=0.006-0.404$ μm, it was shown that the coefficient $\kappa(L)$ grows with L in accord with the power-law dependence. The similar dependence was confirmed in other studies.[25] This conclusion is confirmed completely by our analysis, so that we observe that the power law is observed for nanotubes with any chirality, but the growth rate depends on the nanotube diameter: the larger the diameter, the slower the growth of thermal conductivity.

The analysis of experimental and numerical studies presented in Ref. 28 leads to the conclusion that at room temperatures the thermal conductivity is proportional to the nanotube diameter (for SWCNTs) or squared diameter (for multiwall nanotubes). Our results do not confirm these conclusions and, as follows from Fig. 11, such dependencies are valid for short nanotubes only. The second important conclusion[28] that the nanotubes demonstrate is the ballistic-diffusive regime of thermal conductivity with the coefficient κ depending on the length as L^α, where $\alpha=0.8$ for the room temperature. Our results confirm the power-law growth of the thermal conductivity coefficient, but the exponent α is fund to depend on the nanotube diameter (see Fig. 11) and α decreases monotonically with the diameter. We also mention that the experiments of the electric transport of nanotubes[37] came to the same conclusion about the ballistic-diffusive mechanism of the heat transfer.

Dynamics of a heat pulse in a SWCNT was studied in Ref. 29. Numerical results demonstrated that the pulse

propagates as a wave and the long-wave acoustic phonons contribute into the ballistic energy flux. As the results, the SWCNT demonstrates an infinite conductivity, the result which is confirmed by our analysis presented above. Numerical modeling of the heat pulse propagation in double-well nanotubes (9,0)/(18,0) and (5,5)/(10,10) conducted in Ref. 33 also suggested that the main part of the heat pulse propagates with the sound speed of long-wave acoustic phonons.

The heat transport in SWCNTs with a superlattice of isotopes $^{12}C/^{13}C$ was analyzed in Ref. 30. A direct numerical modeling of the energy transfer demonstrated that the values of the thermal conductivity coefficient depend on the superlattice period. For the nanotube (5,5), it was found a period corresponding to the smallest value of thermal conductivity.

Numerical modeling of the heat transfer in multiwall nanotubes with the external shell with the chirality index (5,5) was carried out in Ref. 34. It was shown that the multiwall nanotube also possesses an infinite thermal conductivity. In this case, the coefficient of thermal conductivity κ grows with L as $\log(L)$.

Last but not least, we mention that all earlier paper studying the thermal conductivity of nanotubes considered only isolated nanotubes, and the effect of substrate has not been discussed in the literature so far to the best of our knowledge.

VIII. SUMMARY AND CONCLUSION

We have studied numerically the thermal conductivity of single-walled carbon nanotubes for the cases of an isolated nanotube and the nanotube interacting with a solid substrate. We have employed two different numerical methods and compared the results for the models with different types of interatomic potentials. Our results have revealed a number of important *general features* of the thermal conductivity and heat transfer in single-walled carbon nanotubes which do not depend much of the type of the interatomic potential used to model the nanotube dynamics as well as on the numerical methods employed for the study of the thermal conductivity and the dependence of the thermal conductivity coefficient on the nanotube length.

In brief, our major results can be summarized as follows.

(1) An isolated infinite ideal single-walled carbon nanotube which is not fixed on a substrate demonstrates *anomalous thermal conductivity*, as was already established in previous numerical studies. In our work, this result has been confirmed by analyzing the dependence of the thermal conductivity coefficient κ on the length L of the nanotube which has been shown to follow the power dependence for large L, $\kappa \sim L^{\beta}$ with $\beta > 0$, and the power dependence of the correlation function, $C(t) \sim t^{\alpha}$ with $0 < \alpha < 1$ for $t \to \infty$. The exponents α and β depend only on the nanotube radius R but not on the chirality index. For larger R, the value of α grows but β decreases.

(2) Our extensive numerical studies of the dependence of the thermal conductivity coefficient on temperature have revealed that the carbon nanotube demonstrates similar anomalous thermal conductivity for all temperatures in the range $T \leq 500$ K.

(3) We have reveled that the interaction of the carbon nanotube with a substrate may change dramatically the character of its thermal conductivity due to both the appearance of a narrow gap in the frequency spectrum associated with long-wave acoustic phonons as well as absorption of acoustic phonons by the substrate.

We believe these results may be useful for resolving a number of controversies between earlier numerical simulations and the data of the recent experiments conducted with nanotubes placed on a substrate.

ACKNOWLEDGMENTS

The authors acknowledge the support of the Australian Research Council and thank the Joint Supercomputer Center of the Russian Academy of Sciences for using their computer facilities. A.V.S. thanks the Center for Nonlinear Studies of the Hong Kong Baptist University and Nonlinear Physics Center at the Australian National University for hospitality and support.

[1] G. W. C. Kaye and T. H. Laby, *Tables of Physical and Chemical Constants* (Longman, London, 1995).
[2] S. Iijima, Nature (London) **354**, 56 (1991).
[3] J. Hone, M. Whitney, C. Piskoti, and A. Zettl, Phys. Rev. B **59**, R2514 (1999).
[4] R. Saito, G. Dresselhaus, and M. S. Dresselhaus, *Physical Properties of Carbon Nanotubes* (Imperial College Press, London, 1998).
[5] A. Jorio, G. Dresselhaus, and M. S. Dresselhaus, *Carbon Nanotubes: Advanced Topics in the Synthesis, Structure, Properties and Applications* (Springer-Verlag, Berlin, 2008).
[6] A. Javey, P. Qi, Q. Wang, and H. Dai, Proc. Natl. Acad. Sci. U.S.A. **101**, 13408 (2004).
[7] B. A. Cola, X. Xu, and T. S. Fisher, Appl. Phys. Lett. **90**, 093513 (2007).
[8] K. Zhang, Y. Chai, M. M. F. Yuen, D. G. W. Xiao, and P. C. H. Chan, Nanotechnology **19**, 215706 (2008).
[9] E. Pop, D. Mann, J. Cao, Q. Wang, K. Goodson, and H. Dai, Phys. Rev. Lett. **95**, 155505 (2005).
[10] P. Kim, L. Shi, A. Majumdar, and P. L. McEuen, Phys. Rev. Lett. **87**, 215502 (2001).
[11] M. Fujii, X. Zhang, H. Xie, H. Ago, K. Takahashi, T. Ikuta, H. Abe, and T. Shimizu, Phys. Rev. Lett. **95**, 065502 (2005).
[12] Tae Y. Choi, D. Poulikakosa, J. Tharian, and U. Sennhauser, Appl. Phys. Lett. **87**, 013108 (2005).
[13] E. Brown, L. Hao, J. C. Gallop, and J. C. Macfarlane, Appl. Phys. Lett. **87**, 023107 (2005).
[14] C. Yu, L. Shi, Z. Yao, D. Li, and A. Majumdar, Nano Lett. **5**, 1842 (2005).
[15] E. Pop, D. Mann, Q. Wang, K. Goodson, and H. Dai, Nano Lett.

6, 96 (2006).
[16] T.-Y. Choi, D. Poulikakos, J. Tharian, and U. Sennhauser, Nano Lett. **6**, 1589 (2006).
[17] C. W. Chang, D. Okawa, H. Garcia, A. Majumdar, and A. Zettl, Phys. Rev. Lett. **99**, 045901 (2007).
[18] S. Berber, Y.-K. Kwon, and D. Tomanek, Phys. Rev. Lett. **84**, 4613 (2000).
[19] J. Che, T. Cagin, and W. A. Goddard III, Nanotechnology **11**, 65 (2000).
[20] S. Maruyama, Physica B **323**, 193 (2002).
[21] D. J. Yang, Q. Zhang, G. Chen, S. F. Yoon, J. Ahn, S. G. Wang, Q. Zhou, Q. Wang, and J. Q. Li, Phys. Rev. B **66**, 165440 (2002).
[22] S. Maruyama, Nanoscale Microscale Thermophys. Eng. **7**, 41 (2003).
[23] W. Zhang, Z. Zhu, F. Wang, T. Wang, L. Sun, and Z. Wang, Nanotechnology **15**, 936 (2004).
[24] M. Grujicic, G. Cao, and W. N. Roy, J. Mater. Sci. **40**, 1943 (2005).
[25] G. Zhang and B. Li, J. Chem. Phys. **123**, 114714 (2005).
[26] Z. Yao, J.-S. Wang, B. Li, and G.-R. Liu, Phys. Rev. B **71**, 085417 (2005).
[27] G. Wu and J. Dong, Phys. Rev. B **71**, 115410 (2005).
[28] J. Wang and J.-S. Wang, Appl. Phys. Lett. **88**, 111909 (2006).
[29] J. Shiomi and S. Maruyama, Phys. Rev. B **73**, 205420 (2006).
[30] J. Shiomi and S. Maruyama, Phys. Rev. B **74**, 155401 (2006).
[31] S. Maruyama, Y. Igarashi, Y. Taniguchi, and J. Shiomi, J. Therm. Sci. Technol. **1**, 138 (2006).
[32] D. Donadio and G. Galli, Phys. Rev. Lett. **99**, 255502 (2007).
[33] T. Kim, M. A. Osman, C. D. Richards, D. F. Bahr, and R. F. Richard, Phys. Rev. B **76**, 155424 (2007).
[34] G. Wu and B. Li, Phys. Rev. B **76**, 085424 (2007).
[35] J. Shiomi and S. Maruyama, Jpn. J. Appl. Phys. **47**, 2005 (2008).
[36] J. Shiomi and S. Maruyama, Int. J. Thermophys. (2009) online. DOI: 10.1007/s10765-008-0516-8
[37] H.-Y. Chiu, V. V. Deshpande, H. W. Ch. Postma, C. N. Lau, C. Miko, L. Forro, and M. Bockrath, Phys. Rev. Lett. **95**, 226101 (2005).
[38] Z. L. Wang, D. W. Tang, X. B. Li, X. H. Zheng, W. G. Zhang, L. X. Zheng, Y. T. Zhu, A. Z. Jin, H. F. Yang, and C. Z. Gu, Appl. Phys. Lett. **91**, 123119 (2007).
[39] D. W. Brenner, Phys. Rev. B **42**, 9458 (1990).
[40] D. W. Brenner, O. A. Shenderova, J. A. Harrison, S. J. Stuart, B. Ni, and S. B. Sinnott, J. Phys.: Condens. Matter **14**, 783 (2002).
[41] C. Li and T.-W. Chou, Int. J. Solids Struct. **40**, 2487 (2003).
[42] Y. Jin and F. G. Yuan, Compos. Sci. Technol. **63**, 1507 (2003).
[43] R. F. Gibson, E. O. Ayorinde, and Y.-F. Wen, Compos. Sci. Technol. **67**, 1 (2007).
[44] D. W. Noid, B. G. Sumpter, and B. Wunderlich, Macromolecules **24**, 4148 (1991).
[45] B. G. Sumpter, D. W. Noid, G. L. Liang, and B. Wunderlich, Adv. Polym. Sci. **116**, 27 (1994).
[46] A. V. Savin and L. I. Manevitch, Phys. Rev. B **58**, 11386 (1998); Phys. Rev. E **61**, 7065 (2000); Phys. Rev. B **67**, 144302 (2003).
[47] A. V. Savin and Yu. S. Kivshar, EPL **82**, 66002 (2008).
[48] R. Al-Jishi and G. Dresselhaus, Phys. Rev. B **26**, 4514 (1982).
[49] T. Aizawa, R. Souda, S. Otani, Y. Ishizawa, and C. Oshima, Phys. Rev. B **42**, 11469 (1990).
[50] R. Kubo, M. Toda, and N. Hashitsume, Springer Ser. Solid-State Sci. **31**, 185 (1991).
[51] N. G. Chopra, L. X. Benedict, V. H. Crespl, M. L. Cohen, S. G. Loule, and A. Zettl, Nature (London) **377**, 135 (1995).
[52] G. Gao, T. Cagin, and W. A. Goddard III, Nanotechnology **9**, 184 (1998).
[53] B. Liu, M.-F. Yu, and Y. Huang, Phys. Rev. B **70**, 161402(R) (2004).
[54] S. Lepri, R. Livi, and A. Politi, Phys. Rep. **377**, 1 (2003).
[55] J. Hone, M. C. Llaguno, N. M. Nemes, A. T. Johnson, J. E. Fischer, D. A. Walters, M. J. Casavant, J. Schmidt, and R. E. Smalley, Appl. Phys. Lett. **77**, 666 (2000).
[56] V. N. Popov, Phys. Rev. B **66**, 153408 (2002).
[57] J. X. Cao, X. H. Yan, Y. Xiao, Y. Tang, and J. W. Ding, Phys. Rev. B **67**, 045413 (2003).
[58] I. M. Lifshitz, Zh. Eksp. Teor. Fiz. **22**, 471 (1952).
[59] W. Yi, L. Lu, Z. Dian-lin, Z. W. Pan, and S. S. Xie, Phys. Rev. B **59**, R9015 (1999).
[60] A. Mizel, L. X. Benedict, M. L. Cohen, S. G. Louie, A. Zettl, N. K. Budraa, and W. P. Beyermann, Phys. Rev. B **60**, 3264 (1999).
[61] C. Dames and G. Chen, Appl. Phys. Lett. **87**, 031901 (2005).